J. Fluid Mech. (2004), *vol.* 503, *pp.* 93–124.
DOI: 10.1017/S0022112003007584 Printed in the United Kingdom

Relative dispersion in isotropic turbulence. Part 1. Direct numerical simulations and Reynolds-number dependence

By P. K. YEUNG[1] AND MICHAEL S. BORGAS[2]

[1]School of Aerospace Engineering, Georgia Institute of Technology, Atlanta, GA 30332, USA
yeung@peach.ae.gatech.edu

[2]CSIRO Atmospheric Research, Private Bag no. 1, Aspendale, VIC 3195, Australia
michael.borgas@csiro.au

(Received 9 August 2002 and in revised form 22 September 2003)

The relative dispersion of fluid particle pairs in isotropic turbulence is studied using direct numerical simulation, in greater detail and covering a wider Reynolds number range than previously reported. A primary motivation is to provide an important resource for stochastic modelling incorporating information on Reynolds-number dependence. Detailed results are obtained for particle-pair initial separations from less than one Kolmogorov length scale to larger than one integral length scale, and for Taylor-scale Reynolds numbers from about 38 to 230. Attention is given to several sources of uncertainty, including sample size requirements, value of the one-particle Lagrangian Kolmogorov constant, and the temporal variability of space-averaged quantities in statistically stationary turbulence.

Relative dispersion is analysed in terms of the evolution of the magnitude and angular orientation of the two-particle separation vector. Early-time statistics are consistent with the Eulerian spatial structure of the flow, whereas the large-time behaviour is consistent with particle pairs far apart moving independently. However, at intermediate times of order several Kolmogorov time scales, and especially for small initial separation and higher Reynolds numbers, both the separation distance and its rate of change (called the separation speed) are highly intermittent, with flatness factors much higher than those of Eulerian velocity differences in space. This strong intermittency is a consequence of relative dispersion being affected by a wide range of length scales in the turbulent flow as some particle pairs drift relatively far apart. Numerical evidence shows that substantial dispersion occurs in the plane orthogonal to the initial separation vector, which implies that the orientation of this vector has, especially for small initial separation, only limited importance.

1. Introduction

It is well known that efficient dispersion is a primary characteristic of turbulence that is best studied from a Lagrangian viewpoint (Batchelor 1952), via the relative motion of fluid elements on average moving apart from each other in an irregular manner. Indeed, for a given source distribution in space, the basic principles for using knowledge of the motion of fluid particles considered singly and in pairs to calculate respectively the mean and variance of the concentration field are well known (Sawford 1985; Thomson 1987, 1990). Lagrangian statistical models of fluid particle motion based on these considerations are an essential component in air-quality science

concerned with the transport of pollutants in the atmospheric environment (e.g. Weil, Sykes & Venkatram 1992; Physick & Hurley 1994). However, the modelling of 'two-particle' statistics for relative dispersion is considerably more complex than that for corresponding 'one-particle' quantities (where each particle in a 'cloud' is treated independently). Work on two-particle relative dispersion was reviewed by Sawford (2001). Improved understanding at a quantitative level is essential for the development of better models.

This paper is Part 1 of a coordinated effort to use direct numerical simulations (DNS) of turbulence to study relative dispersion over a range of Reynolds numbers, and to develop a new stochastic model (Borgas & Yeung 2004, hereinafter referred to as Part 2). Despite recent advances in experiments (Voth, Satyanarayanan & Bodenschatz 1998; Ott & Mann 2000; La Porta *et al.* 2001; Mordant *et al.* 2001), DNS is still the most detailed source of Lagrangian data in turbulence (e.g. Yeung & Pope 1989; Kimura & Herring 1996; Yeung 2001). On the other hand, because of Reynolds-number limitations in DNS, accurate parameterization of Reynolds-number effects is very important. This consideration is especially crucial for dispersion models developed with the aid of DNS data but ultimately intended for application to high-Reynolds-number flows such as those in the atmospheric environment (Sawford *et al.* 2003).

In general, a complete description of the motion of a pair of fluid particles, here labelled by superscripts $^{(1)}$ and $^{(2)}$, requires knowledge of well-resolved time histories of their instantaneous positions (i.e. $\boldsymbol{x}^{(1)}(t)$ and $\boldsymbol{x}^{(2)}(t)$). However, if the turbulence is homogeneous, or if inhomogeneity is weak within the region of travel of these particles, it is sufficient to consider the statistics of the separation vector $\boldsymbol{l}(t) \equiv \boldsymbol{x}^{(1)}(t) - \boldsymbol{x}^{(2)}(t)$. Furthermore, it is clear that if isotropy also applies then much of the essential physics would be captured in the magnitude of the separation vector, with the vector orientation relative to fixed coordinate axes being much less important. It may be recognized that most pollutant sources, such as chimneys in the atmosphere, are small compared to the macroscopic length scales of the flow. Use of classical concepts of local isotropy then suggests that there may be strong similarities in early-time behaviour between dispersion in isotropic and anisotropic turbulent flows. This consideration gives further justification for using the simplified case of isotropic turbulence as a testbed for both physical understanding and model development.

As suggested above, for relative dispersion in isotropic turbulence, the most fundamental variable is the separation distance, $l \equiv |\boldsymbol{l}|$, at any given elapsed time evolving from a specified initial separation (l_0). The rate at which the particle pairs move apart on average is given by the rate of growth of the mean separation distance, $\langle l \rangle$, which is averaged over an ensemble of particle pairs with the same initial separation. Clearly, it is useful to study the statistics of the time derivative $\mathrm{d}l/\mathrm{d}t$, here called the *separation speed* (u_r) which is the projection of the relative velocity ($\boldsymbol{u}^{(r)}$) along the direction of the separation vector, i.e.

$$\mathrm{d}l/\mathrm{d}t = u_r \equiv \left(\boldsymbol{u}^{(r)} \cdot \boldsymbol{l}\right)/l, \tag{1}$$

where $\boldsymbol{u}^{(r)} \equiv \boldsymbol{u}^{(1)} - \boldsymbol{u}^{(2)}$, with $\boldsymbol{u}^{(1)}, \boldsymbol{u}^{(2)}$ being the velocities of individual particles in each pair. The dot product in (1) implies that angular orientation is important. In particular, the angle between the vectors $\boldsymbol{u}^{(r)}$ and $\boldsymbol{l}$, denoted by θ_1, determines the sign of u_r, and is more likely to be acute than obtuse. In addition, we also consider the angle between $\boldsymbol{l}(t)$ and $\boldsymbol{l}(0)$, denoted by θ_2, which measures the change in angular orientation of $\boldsymbol{l}(t)$ over time t. If θ_2 changes rapidly from its initial value of zero, then it would imply that the orientation of the initial separation vector is, perhaps even

in anisotropic turbulence, relatively unimportant. The stretching of the separation distance (as reflected by (1)) and the rotation of the separation vector (measured by θ_2) are two distinct processes which must be considered for effective relative dispersion modelling.

Whereas the quantities $\boldsymbol{u}^{(r)}$ and u_r are inherently Lagrangian, as velocity differences sampled between two (moving) points in space, their statistical properties are strongly influenced by the spatial structure of the flow. Other investigators (e.g. Chertkov, Pumir & Shraiman 1999; Frisch *et al.* 1999; Gat, Procaccia & Zeitak 1998) have used the motion of multi-particle clusters (involving two particles or more) as a tool for probing important aspects of spatial structure in turbulence. It is crucial that appropriate Eulerian structural information be included in models of relative dispersion in a rational manner. These considerations have also motivated recent use (Fung & Vassilicos 1998; Malik & Vassilicos 1999) of the technique of kinematic simulations (KS, see Fung *et al.* 1992) in which modelled flow fields are constructed mathematically to consist of several types of structural regions ('streaming', 'straining', 'eddying') believed to mimic those found in actual turbulent flows. Specifically, in the present context 'streaming' regions are those where particle pairs largely move together with little relative velocity, 'straining' regions are where the particles are pulled apart from each other by local strain fields giving a large separation speed, whereas 'eddying' regions are where the relative motion is largely orthogonal to the separation vector thus contributing little to the separation speed. Straining and eddying regions can be characterized in terms of the angle θ_1 defined above, as θ_1 being close to 0° (and acute) and close to 90°, respectively. We can also diagnose straining, streaming and eddying based on l and θ_2: with little rotation or stretching in streaming regions; strong stretching and a jump in θ_2 in straining regions; and weak stretching and persistent growth of θ_2 indicating rotation in eddying regions.

Part of the complexity of relative dispersion is that, as the particle pairs move apart (on average), they become exposed to the effects of velocity fluctuations over an increasingly wide range of scale sizes. This is especially true for particle pairs of small initial separation and at intermediate times much larger than the Kolmogorov time scale (τ_η), but yet much smaller than the Lagrangian integral time scale (T_L) of the velocity fluctuations. In this regime, the relative separation process is strongly accelerating, with both $\langle l \rangle$ and $\langle u_r \rangle$ (averaged over all particle pairs of fixed l_0) increasing rapidly in time. Previous results at lower Reynolds number (Yeung 1994) show that in this phase, both the separation and the relative velocity are highly intermittent, with non-Gaussian skewness and flatness factors. The probability density function (p.d.f.) of l has a very strong positive skewness, meaning that there are times when a small number of particle pairs have drifted apart while the majority are still close together. The high flatness factor of the relative velocity observed in DNS was given much attention in the kinematic simulation study by Malik & Vassilicos (1999). We would expect these intermittency properties to be more pronounced at higher Reynolds number; results in this paper show that indeed they are. However, the indications are that the peak intermittency properties are a consequence of dissipation range, or explicit viscous effects (which retard separation) rather than just the accelerating separation process which persists throughout the dissipation and inertial ranges of turbulent fluctuations.

In this paper, we focus on relative dispersion in stationary isotropic turbulence, primarily via statistics of the quantities l, u_r, θ_1 and θ_2. Some of these quantities were previously studied at lower Reynolds number (Yeung 1994), and some results on θ_1 and θ_2 were given in Yeung & Borgas (1998). Brief results from DNS at

higher Reynolds number have also been reported by Ishihara & Kaneda (2002), who have emphasized inertial-range scaling properties suggested by Richardson (1926). However, detailed data at several Reynolds numbers ($R_\lambda \approx 38$, 90, 140 and 230 based on the Taylor scale) currently available at grid resolutions from 64^3 to 512^3 now allow us to examine issues of Reynolds-number dependence with greater rigour than before. Special attention is given here to quantities with a direct role in the model formulation as described in Part 2. We also discuss statistical sampling issues for Lagrangian quantities, which become more demanding at higher Reynolds number.

The remaining sections of this paper are organized as follows. In § 2, we briefly review the numerical methods employed in DNS, including Eulerian flow parameters and statistical considerations in the data analysis. In § 3, we discuss related results on the one-particle Lagrangian velocity structure function, with emphasis on the Lagrangian Kolmogorov constant (C_0) which is a key model parameter. Two-particle results are given in § 4, including p.d.f.s and statistical moments which can be compared with dispersion models. Separate subsections are devoted to the statistics of separation distance, and the separation speed incorporating issues of vectorial alignment. Reynolds-number effects are discussed throughout. Finally, in § 5, we summarize the results and discuss their implications for modelling.

2. Numerical simulation and data analysis

2.1. *Simulation method and parameters*

The DNS approach we use is based on the Fourier pseudospectral method of Rogallo (1981), with second-order differencing in time and particle-tracking (Yeung & Pope 1988). We consider isotropic turbulence made statistically stationary in time by random forcing at the large scales (Eswaran & Pope 1988). Cubic-spline interpolation is used to obtain the Lagrangian fluid particle velocity from the Eulerian velocity field at instantaneous particle positions. Several accuracy requirements for the extraction and processing of Lagrangian data are addressed in Yeung (2002).

The study of relative dispersion in DNS requires careful choices for the initial separation vectors, denoted by $\boldsymbol{l}(0)$. Since our solution domain is a cube it is natural to choose equal numbers of samples of $\boldsymbol{l}(0)$ aligned with each coordinate axis. To enhance statistical accuracy, it is also desirable to arrange initial particle locations in a manner which gives a larger number of particle pairs (of selected $l_0 \equiv |\boldsymbol{l}(0)|$) while optimizing the degree of statistical independence among these samples. In Yeung (1997*a*), the initial configuration consists of sets of tetrahedra, each yielding three particle pairs with initial separation vectors given by

$$\boldsymbol{l}(0) = (\pm l_0, 0, 0), \quad (0, \pm l_0, 0) \quad \text{or} \quad (0, 0, \pm l_0). \tag{2}$$

We use a slight variation of this scheme, whereby improved flexibility in ensemble size is achieved by allowing the base vertices of these tetrahedra to be located randomly in space instead of being arranged as a cubic lattice. Because the simulated turbulence is stationary, the choice of time origin is in principle unimportant. Nevertheless, before releasing the fluid particles, we do allow sufficient time (about 4 eddy-turnover times for the 512^3 simulation) for a satisfactory stationary state to emerge, free of artefacts associated with difficulties of choosing initial conditions representative of fully developed turbulence.

The DNS results reported in this paper are obtained from simulations at 64^3, 128^3, 256^3 and 512^3 grid resolutions, with Reynolds numbers corresponding to those in Yeung (2001) which focused on one-particle statistics of velocity and passive scalar

Grid	128^3	256^3	512^3
R_λ	89	141	230
$k_{max}\eta$	1.51	1.41	1.39
L_1/η	56	101	193
T_L/τ_η	8.5	12.9	19.8
T_L/T_E	0.72	0.76	0.76

TABLE 1. Summary of selected numerical simulation parameters.

fields. For convenience some of the major parameters including Reynolds number and length- and time-scale ratios are given in table 1. The 512^3 data are (see Yeung & Zhou 1997) at sufficiently high Reynolds number to show limited inertial range behaviour in the energy spectrum with a Kolmogorov constant in good agreement with experiments (Sreenivasan 1995). In each case, the initial separation ranges from 1/4 of the Kolmogorov length scale (η) to a value that is greater than the size of the large scales (measured by the integral length scale L_1) in the flow. The same degree of small-scale resolution is maintained uniformly for all simulations by having the parameter $k_{max}\eta$ (where k_{max} is the highest wavenumber resolved by the grid) being close to 1.5. As expected, the range of length scales simulated increases with Reynolds number, while the increase in time-scale ratio (T_L/τ_η) is quite modest. (The implications of this for the attainment of Reynolds-number similarity in Lagrangian statistics are discussed in Yeung 2002.) Consistent with a trend of increasing intermittency, we find that, for a given number of particle pairs, the magnitude of statistical errors increases with Reynolds number. In the 512^3 simulation (which gives the highest Reynolds number reported here), we have tracked 24 576 particle pairs for each choice of l_0. However, in view of the sampling requirements discussed in § 2.2 below, to obtain better results at early times we have also tracked eight times as many (196 608) particle pairs of initial separations $l_0/\eta = 1/4$, 1 and 4 for a time period up to $20\tau_\eta$.

2.2. *Statistical sampling*

Accurate sampling for one- and two-particle statistics requires a sufficiently large ensemble of fluid particles and particle pairs, whose initial positions should be chosen to give a high degree of statistical independence among the samples. In practice, some uncertainty in the results is inevitable. For relative dispersion, an inherent source of difficulty lies in the strongly intermittent character of the process, which is especially evident for high-order moments at intermediate times for particle pairs of small initial separation. In our simulations, the stochastic character of the forcing scheme is also a contributing factor. The overall uncertainty can be strong enough to cause ambiguities in the interpretation of Reynolds-number effects, say between data at one Reynolds number and the next higher value. To ensure the reliability of our results, it is important to develop systematic estimates of statistical error, and to understand how they depend on the simulation parameters.

The main idea involved is to divide the particle- and particle-pair data into (say) M subensembles of equal size, calculate statistics for each subensemble, and finally to estimate confidence intervals using standard techniques, as below. We denote by X a generic statistical variable (such as skewness or flatness of the separation distance), for which each subensemble is regarded as providing one sample value. The primary issue is how closely the theoretical mean value $\overline{X}$ is approximated by the sample mean μ from these M measurements of X, in terms of the standard deviation σ.

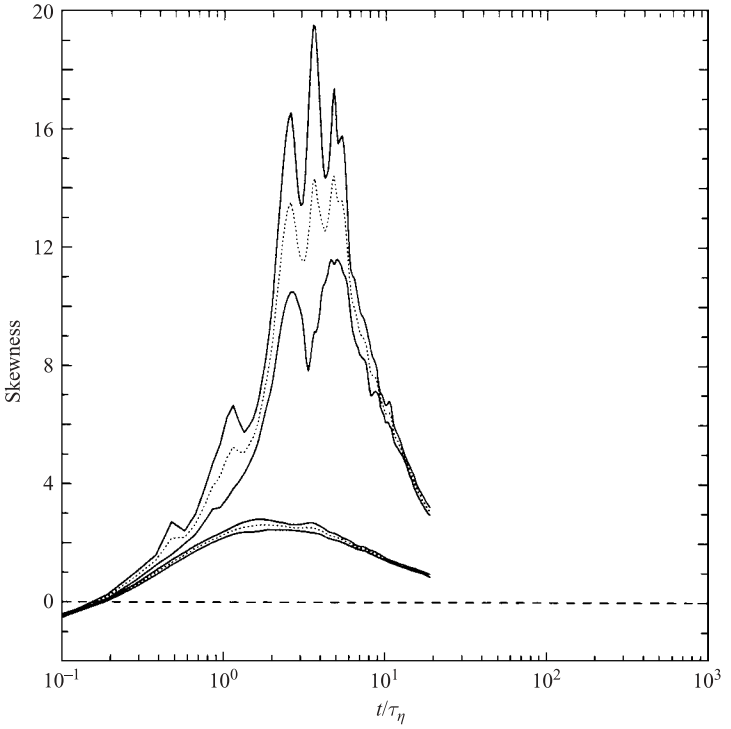

FIGURE 1. Statistical variability in skewness of u_r in 512^3 DNS data, measured by $\pm 95\%$ confidence intervals (solid lines) computed from 8 subensembles, centred on the overall mean value (dashed lines) from 196 608 particle pairs. Upper curves for $l_0/\eta = 1/4$, lower curves for $l_0/\eta = 4$.

Following classical distribution theory (e.g. Bickel & Doksum 1977), we suppose that the variable $Y \equiv (\overline{X} - \mu)\sqrt{M}/\sigma$ behaves according to a Student's t distribution of M degrees of freedom. (This assumption is not rigorous if X is not Gaussian; however, it is necessary to allow progress in the analysis.) We can then obtain statistical bounds on X by, for instance, the inequality

$$t_5 < \frac{(\overline{X} - \mu)\sqrt{M}}{\sigma} < t_{95}, \tag{3}$$

where t_5 and t_{95} are, respectively, the 5th and 95th percentiles of the Student's t distribution. (Note that the symmetry of this distribution implies $t_5 = -t_{95}$.) Effectively, we suppose that $\overline{X}$ lies within the 'confidence interval' $\mu \pm \sigma t_{95}/\sqrt{M}$ with 90% probability. Clearly, the size of the confidence interval gives a measure of the statistical error involved in the estimate of μ, decreasing as $M^{-1/2}$. For $M > 30$, the t distribution becomes nearly the same as Gaussian, as we would expect by application of the central limit theorem.

Figure 1 shows the magnitudes of 95% confidence intervals for the skewness of separation speed (u_r) in the 512^3 simulations with l_0/η being 1/4 and 4. A total of 196 608 particle pairs are tracked for a period of $20\tau_\eta$ and divided into 8 subensembles for error analysis. It is clear that statistical errors are much larger for small initial separations. Furthermore, they are largest at intermediate times of peak skewness, (when the distribution of separation distances has the widest spread in a relative sense, measured by standard deviation normalized by the mean), but decrease rapidly

at later times. These data trends also imply that statistical variability among the subensembles (each of 24 576 pairs) would be insignificant at times later than $20\tau_\eta$ for small l_0, and at all times for our next larger choice of l_0 (16η). Consequently, we conclude that the statistical accuracy obtained from the use of 196 608 pairs of small l_0 at early times combined with 24 576 pairs for the rest of the data range is sufficient for the 512^3 DNS results in this paper.

It may be noted that, although the use of confidence intervals in turbulence statistics is by no means new (e.g. Overholt & Pope 1996), error estimates at this level of rigour in respect of the particle (or particle-pair) ensemble size are rarely available in the literature. However, this is important for results from DNS, kinematic simulations and stochastic modelling alike. In our work, the analysis of subensemble datasets is conveniently performed by a parallel post-processing code which obtains overall statistics by collecting results from multiple processors. This approach of subensemble processing also facilitates the analysis of large-volume Lagrangian datasets which exceed most single-processor memory capacities.

2.3. *Variability of global parameters*

It is well known that different forcing schemes (see Overholt & Pope 1998) used in simulations of stationary isotropic turbulence give rise to different levels of temporal variability of globally averaged statistics (e.g. turbulence kinetic energy K and its mean dissipation rate $\langle\epsilon\rangle$). The variability of ϵ which is used in discussions of Kolmogorov similarity and stochastic model implementation requires special attention.

Our results in this work are, for each grid resolution, derived from a single simulation of turbulent flow within a finite domain in space and over a finite interval in time, subjected to random forcing at the large scales. This amounts to a single realization of the flow field in each case. In principle, better statistics can be obtained by performing multiple simulations and averaging over those, but, in general, practical computing constraints do not readily allow for such an approach. Consequently, when considering the scaling of Lagrangian statistics, there is a risk of significant bias if the value of ϵ averaged over a particular *epoch* deviates substantially (say 25% or more) from the long-time average. In principle, the uncertainties can be greatly reduced by tracking different ensembles of particles and particle pairs over different epochs, and by subsequently averaging over results obtained over such different epochs. However, this is cumbersome and impractical when the overall duration of the simulation is limited by high computational costs.

The degree of variability is readily illustrated in figure 2, which shows the evolution of space-averaged K and ϵ within the 512^3 simulation which provided much of the data in this paper. Significant variations are indeed evident within the simulation time period, which is approximately $200\tau_\eta$ in length. Fluctuations are of the order $\pm 25\%$ or more of the time-averaged value, and the largest observed value of ϵ is nearly 80% larger than the smallest. The time scale for the variation of the large-scale randomness is of the order of K/ϵ; from figure 2, we can observe two or three peaks and troughs for the duration of the simulation. In previous work (Yeung & Pope 1989, Appendix A therein) the nature of the forcing scheme we use (Eswaran & Pope 1988) has been identified as the source of much of the observed variability. It is possible is reduce (but not eliminate) this variability by forcing a larger number of Fourier modes within a larger spherical shell in wavenumber space; however, doing so would also lead to a reduction in the Reynolds number achieved.

The facts noted above must be borne in mind when we attempt to describe the Reynolds-number dependence of Lagrangian statistics in a quantitative manner. In

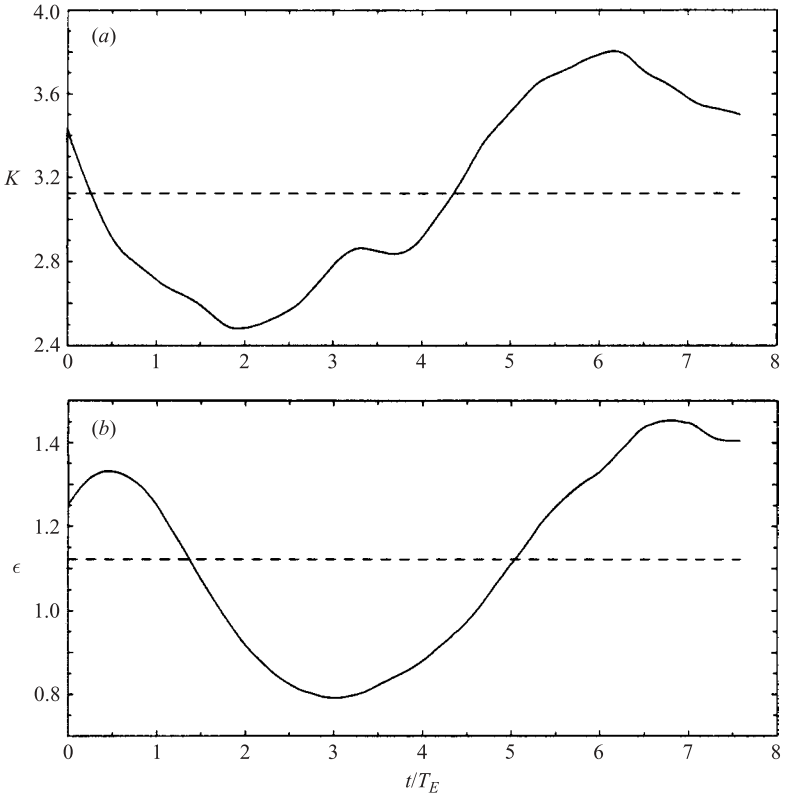

FIGURE 2. Variability in time of spatially averaged quantities in 512^3 simulation: (*a*) turbulence kinetic energy (*b*) energy dissipation rate. Time is normalized by the eddy-turnover time. The dashed horizontal lines shows the respective time averages.

particular, while a long-time average of $\langle\epsilon\rangle$ may still be used for stationary single-particle Lagrangian statistics, for non-stationary two-particle statistics it is appropriate to use a value of $\langle\epsilon\rangle$ averaged over a limited epoch. The value of ϵ at $t=0$ is, in fact, most suitable for assessing scaling relationships at small diffusion times.

3. One-particle Lagrangian structure function

Although our current interests are mainly in two-particle dispersion, knowledge of several one-particle quantities is also an important prerequisite. In principle, one-particle statistics can be estimated from particle-pair datasets by taking only one particle in each pair, or both particles in pairs of large initial separation which gives nearly independent samples. We have found, however, that better one-particle results are obtained by tracking a large collection of particles with randomly distributed initial positions (as in Yeung 2001).

A basic Lagrangian quantity of importance is the velocity increment

$$\Delta_\tau u^+ \equiv u^+(t+\tau) - u^+(t)$$

for a component of velocity (where the superscript $^+$ denotes single-particle quantities) over a time interval τ. Classical inertial scaling (Monin & Yaglom 1975) implies that the second-order Lagrangian velocity structure function (i.e. the mean square of $\Delta_\tau u^+$)

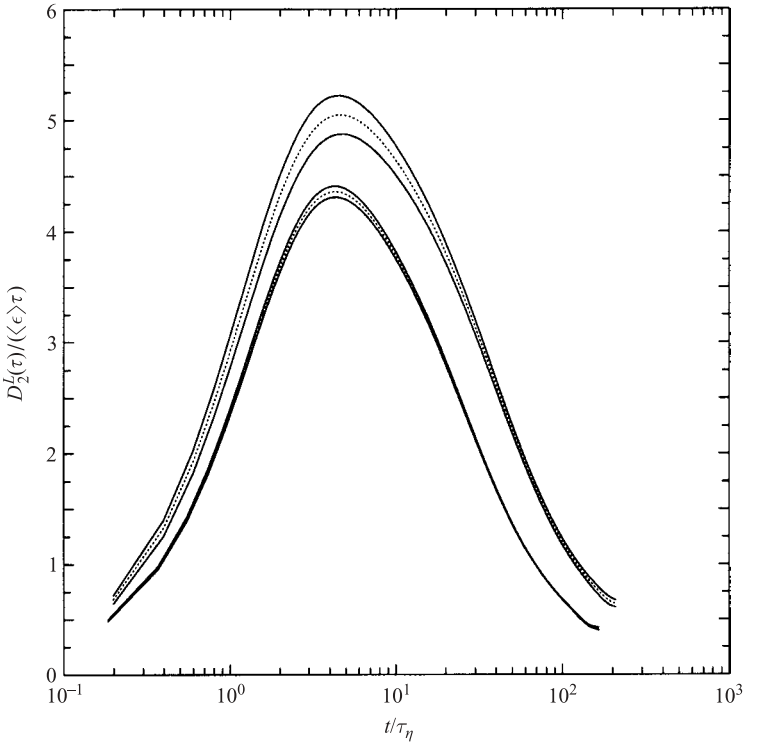

FIGURE 3. Normalized one-particle second-order Lagrangian structure function (dashed lines) with $\pm 95\%$ confidence intervals (solid lines). Upper curves for $R_\lambda = 230$ (512^3), lower curves for $R_\lambda = 140$ (256^3).

has the form

$$D_2^L(\tau) = C_0\langle\epsilon\rangle\tau \quad (\tau_\eta \ll \tau \ll T_L), \tag{4}$$

where $\langle\epsilon\rangle$ is the energy dissipation, and C_0 is the Lagrangian Kolmogorov constant supposed to be universal at high Reynolds number. If an extended inertial range exists, then C_0 can be inferred as the height (C_0^*) of a plateau at intermediate τ by plotting the non-dimensional form $D_2^L(\tau)/(\langle\epsilon\rangle\tau)$. Figure 3 shows such a plot for $R_\lambda = 140$ and 230 from 256^3 and 512^3 simulations, respectively, with confidence intervals estimated using the procedure described in § 2.2. It is clear that, within the Reynolds number range of our simulations, C_0^* has a significant variation, with statistical variability also increasing with Reynolds number.

The value of C_0 is very important in stochastic modelling (see, e.g. Reynolds 1988; Sawford 1991; Du *et al.* 1995; Degrazia & Anfossi 1998), and the issue of its universality is of much current interest (e.g. Heinz 2002; Lien & D'Asaro 2002). It is noteworthy that recent theoretical arguments based on DNS data (Sawford & Yeung 2001; Yeung 2002) have placed the (asymptotic) value of C_0 in the range 6–7. The results seen in figure 3 are not inconsistent with these estimates. Nevertheless, in attempting to compare stochastic model calculations with DNS data at modest Reynolds numbers, it is best (see Sawford & Yeung 2001; Fox & Yeung 2003; Part 2) to replace a constant C_0 by a Reynolds-number-dependent version.

Although in our DNS inertial scaling at intermediate times in the Lagrangian structure function, $D_2^L(\tau)$ is not attained, more rigorous analyses can be made in the limits of small and large time lags. If τ is small, we expect that $D_2^L(\tau)$ will become

proportional to the mean-square fluid particle acceleration $\langle a^{+2}\rangle$. This gives

$$\frac{D_2^L(\tau)}{\langle\epsilon\rangle\tau} \approx a_0\frac{\tau}{\tau_\eta} \quad (\tau \ll \tau_\eta), \tag{5}$$

where $a_0 \equiv \langle a^{+2}\rangle/(\langle\epsilon\rangle^{3/2}\nu^{-1/2})$ is the Kolmogorov-scaled acceleration variance. The Reynolds-number dependence seen at small times in figure 3 reflects the observation in our DNS (Vedula & Yeung 1999) that a_0 increases approximately as $R_\lambda^{1/2}$ within the present Reynolds-number range. (It should be noted that different results have been suggested in the literature – see Voth *et al.* 1998; Hill 2002; Sawford, Borgas & Yeung 2003.) In the other limit of large times, the particle velocities at t and $t+\tau$ become statistically independent. Using standard scaling relations we can show that

$$\frac{D_2^L(\tau)}{\langle\epsilon\rangle\tau} \approx \frac{2\langle u^2\rangle}{\langle\epsilon\rangle\tau} \approx \frac{2}{\sqrt{15}}R_\lambda(\tau/\tau_\eta)^{-1} \quad (\tau \gg T_L), \tag{6}$$

where T_L is the Lagrangian integral time scale (the integral of the one-particle velocity autocorrelation function). Furthermore, since the ratio T_L/τ_η is roughly proportional to R_λ, at higher R_λ, it takes larger values of τ/τ_η to observe large-time behaviour.

For completeness, we also consider briefly here an alternative method for estimating C_0, based on the dispersion of a single fluid particle in an inertial frame moving with the initial particle velocity, i.e. $\boldsymbol{z}^+(t) \equiv \boldsymbol{X}^+(t) - \boldsymbol{X}^+(0) - \boldsymbol{u}^+(0)t$. Classical arguments suggest that the inertial range result for each component of $\boldsymbol{z}^+(t)$ is

$$\langle z^{+2}\rangle = C_0\epsilon t^3 \quad (\tau_\eta \ll t \ll T_L). \tag{7}$$

(It should be noted that this t^3 scaling relation is different from Richardson's scaling for two-particle separation.) Because this relation applies over the time period $\tau_\eta \ll t \ll T_L$, the value of ϵ involved is that averaged over a relatively short period of (say) about 10 τ_η, which (see § 2.3) can be quite different from the global average $\langle\epsilon\rangle$ taken over a long period of time and used in (4). However, this source of uncertainty can be greatly reduced if we divide the entire time series (of length about $200\tau_\eta$ in the 512^3 case) into a number of non-overlapping intervals (of say $10\tau_\eta$ each) and treat these effectively as multiple realizations for the purpose of ensemble averaging.

In figure 4, we compare the normalized quantities $D_2^L(\tau)/\epsilon\tau$ and $\langle z^{+2}\rangle/\epsilon t^3$ where the latter is computed in the manner indicated above and normalized by the global time average $\langle\epsilon\rangle$. It can be seen that the estimates of C_0 from these two quantities are quite close (being 5.05 and 4.95, respectively). The curve based on $\langle z^{+2}\rangle$ appears to 'lag' behind, which is expected because the displacement carries the memory of velocity fluctuations from earlier times. The inset shows the ratio of the two curves in this figure. At small times ($t \ll \tau_\eta$) or over small time intervals ($\tau \ll \tau_\eta$), we can readily show, using Taylor-series expansions, that both $D_2^L(\tau)$ and $\langle z^{+2}\rangle$ are proportional to the fluid particle acceleration variance, such that the ratio shown should have a limiting value of 4/3. Clearly, the sampling procedures we adopted are able to reproduce this limit. On the other hand, we might expect that if a true inertial range exists then this ratio should have a well-defined plateau with a value close to unity, which is not observed in our results. Nevertheless, the apparent consistency between these two estimates of C_0 suggests that the data are approaching a regime of inertial-range similarity behaviour.

Besides numerical simulations, it may be noted that estimates of C_0 have been obtained also in particle-tracking experiments, by Mordant *et al.* (2001) who suggested $C_0 = 3.5$ in flow between counter-rotating disks at $R_\lambda = 740$. This geometry is,

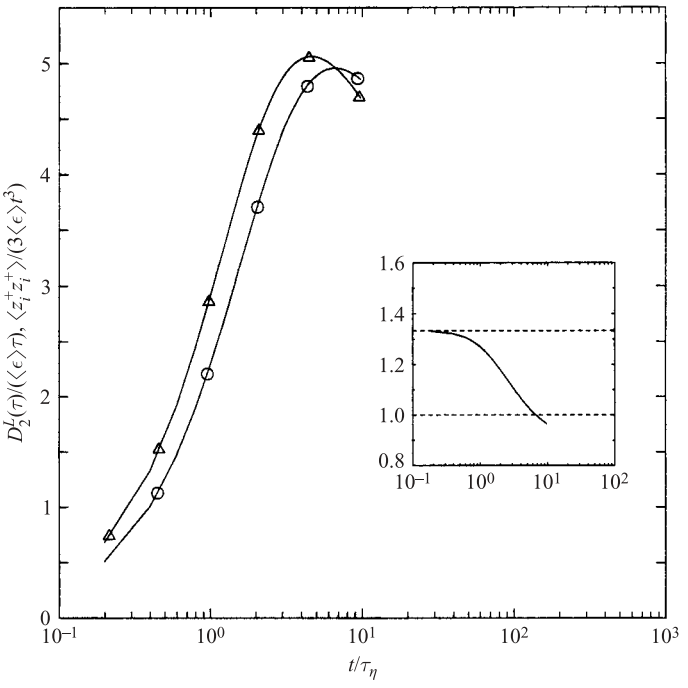

FIGURE 4. Comparison of two normalized quantities for the evaluation of C_0: $D_2^L(\tau)/(\langle\epsilon\rangle\tau)$ ($\triangle$), and $\langle z_i^+ z_i^+\rangle/(3\langle\epsilon\rangle t^3)$($\bigcirc$) at time lags and diffusion times up to $10\tau_\eta$, from 512^3 DNS data. The inset shows the ratio between these two quantities.

incidentally, similar to that in the Lagrangian acceleration measurements by Voth *et al.* (1998). The fact that this value of C_0 seems low compared to DNS remains to be understood.

4. Two-particle statistics

In this section, we present detailed results on relative dispersion from DNS, in part to provide a basis of reference for stochastic model evaluation (Part 2). Results are shown mainly at $R_\lambda = 230$ from a 512^3 simulation, but also at other Reynolds numbers to illustrate the nature of Reynolds-number effects.

4.1. *Separation distance*

In isotropic turbulence, an overall measure of the distance by which fluid particles have moved apart in time is given by the mean-squared relative dispersion $\langle \Delta l_i \Delta l_i \rangle$ where $\Delta \boldsymbol{l} = \boldsymbol{l}(t) - \boldsymbol{l}(0)$. Figure 5 shows the growth of the r.m.s value $\langle \Delta l_i \Delta l_i \rangle^{1/2}$ for a range of initial separations and scaled by the Kolmogorov variables. At early times, i.e. $t \leqslant \tau_\eta$, we observe a period of linear growth (or 'ballistic regime') which is a result of particles moving in straight lines before their velocities have had time to change appreciably. In this limit, each coordinate component Δl_i is proportional to the velocity difference at $t = 0$ measured at points $\boldsymbol{l}(0)$ apart, whose second moments are given by Eulerian structure functions in space. Since $\boldsymbol{l}(0)$ is oriented along a coordinate axis, we can write this result as

$$\langle \Delta l_i \Delta l_i \rangle(t) \approx [D_{LL}(l_0) + 2D_{NN}(l_0)]t^2 (t \ll \tau_\eta), \tag{8}$$

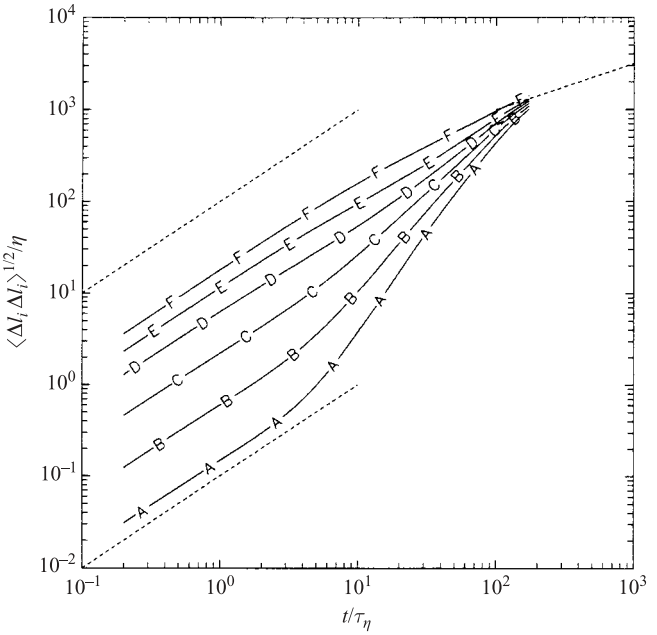

FIGURE 5. Growth of r.m.s relative dispersion $\langle \Delta l_i \Delta l_i \rangle^{1/2}$ (scaled by Kolmogorov variables), from 512^3 DNS with initial separations (lines A–F) $l_0/\eta = 1/4$, 1, 4, 16, 64 and 256. Dashed lines for comparison at small and large times have slopes 1 and 1/2, respectively.

where $D_{LL}(\cdot)$ and $D_{NN}(\cdot)$ are longitudinal and transverse structure functions evaluated here with l_0 as the spatial separation. The spacings between different curves indicate that sensitivity to l_0 becomes weaker for larger l_0 – in fact, if l_0 is made substantially larger than the integral length scale, then the asymptotic small-time behaviour is determined (for line F) only by the single-point velocity variance. In the large-time limit (for $t \gg T_L$) the particle-pair velocities (hence ultimately their displacements) become progressively independent of each other, giving the asymptotic result (Yeung 1994)

$$\langle \Delta l_i \Delta l_i \rangle \approx 4 \langle u_i u_i \rangle T_L t \quad (t \gg T_L), \tag{9}$$

which is indicated by a dashed line of slope 1/2 in the figure. Clearly, it takes longer for particle pairs of small l_0 to approach this asymptote.

Figure 5 is analogous to figure 2 of Yeung (1994), except that a higher Reynolds number is achieved in the current results. At early times, if l_0 is small, then in (8) we can make the substitutions $D_{NN}(l_0) = 2D_{LL}(l_0) = 2 l_0^2 \langle (\partial u/\partial x)^2 \rangle$. Use of the isotropy relation $\langle \epsilon \rangle = 15\nu \langle (\partial u/\partial x)^2 \rangle$ then leads to

$$\frac{\langle \Delta l_i \Delta l_i \rangle^{1/2}}{\eta} \approx \frac{1}{\sqrt{3}} \frac{l_0}{\eta} \frac{t}{\tau_\eta}, \tag{10}$$

which implies universality with respect to Reynolds number and is well satisfied by lines A and B in the figure. This universality does not apply for larger values of l_0 because the structure functions at larger separations will scale more with the integral length scale than the Kolmogorov scale. Reynolds-number effects are more pronounced in the large-time asymptote which reflects the presence of a wider range of scales (for both length and time) in the flow. At higher Reynolds number, this

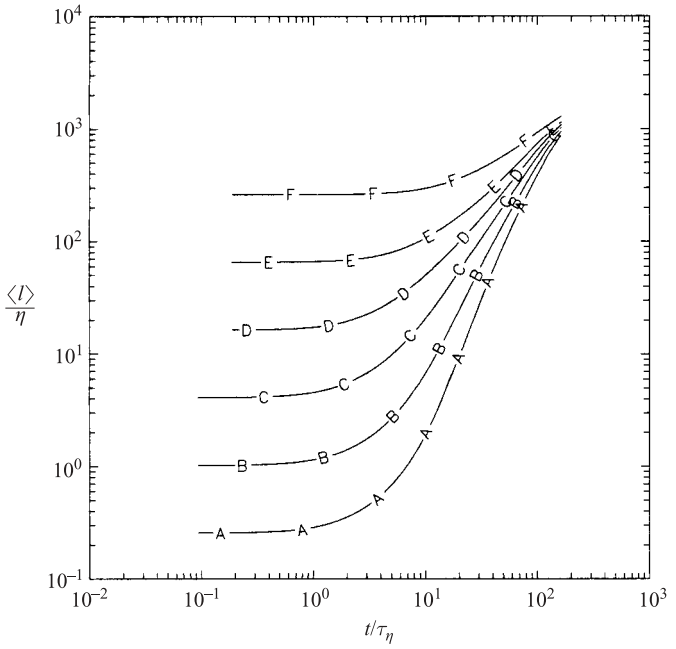

FIGURE 6. Growth of mean separation distance, with same symbols as in figure 5.

large-time asymptote (which is based on T_L) is reached at larger values of t/τ_η, where, of course, the dispersion measured in Kolmogorov scales also increases.

Recent developments in dispersion modelling indicate considerable interest in quasi-one-dimensional models (Kurbanmuradov & Sabelfeld 1995; Part 2; for earlier work see Durbin 1980) in which directional information is suppressed, but instead the separation distance (l) is obtained directly as the solution of a modelled scalar stochastic equation. These models are conceptually simpler and are able to avoid non-uniqueness difficulties associated with evolution equations for vector stochastic processes (Thomson 1987). Consequently, for comparison with quasi-one-dimensional models the moments of l itself are of greater relevance. The first moment, i.e. the mean separation distance, is shown in figure 6 for the same conditions as the data in figure 5. Initially, each curve is nearly flat before changes in l grow in time to a significant fraction of its original value (l_0). However, at later times the behaviour is similar to that seen in figure 5, with data for all choices of l_0 evolving towards $t^{1/2}$ asymptotic growth.

A simple connection between the two measures of dispersion and separation in figures 5 and 6 can be established at later stages in time (occurring earlier for small l_0) when the separation distance becomes much larger than its initial value. In these circumstances it is clear that $\langle \Delta l_i \, \Delta l_i \rangle$ is nearly the same as $\langle l_i l_i \rangle = \langle l^2 \rangle$. As a result, we have

$$\frac{\langle \Delta l_i \, \Delta l_i \rangle}{\langle l \rangle^2} \approx \frac{\langle l^2 \rangle}{\langle l \rangle^2} = 1 + \frac{\sigma_l^2}{\langle l \rangle^2}, \tag{11}$$

which implies that the square of the ratio between the quantities plotted in figures 5 and 6 (on the left-hand side) can be expressed in terms of the ratio of standard deviation (σ_l) to the mean ($\langle l \rangle$) for the separation distance.

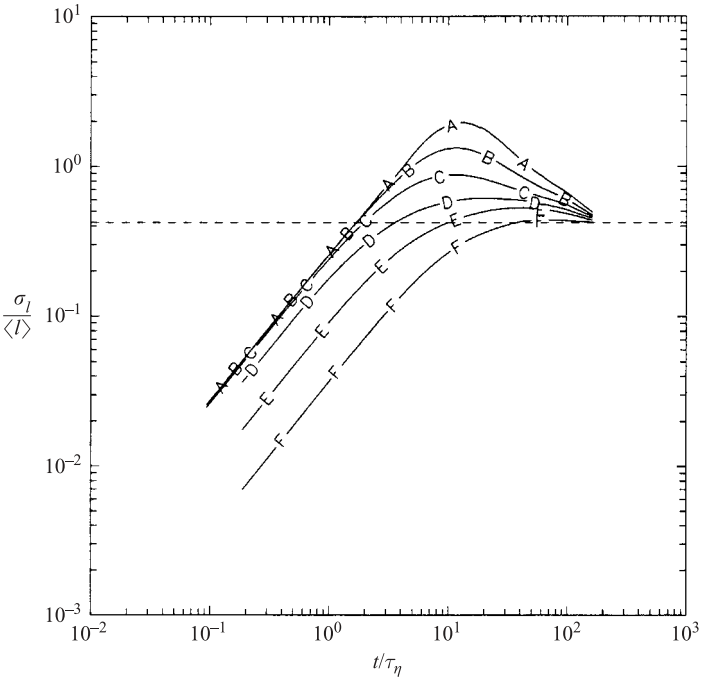

FIGURE 7. Ratio of standard deviation to the mean of separation distance, with same symbols as in figure 5.

Figure 7 shows the evolution of the ratio $\sigma_l/\langle l \rangle$. It can be seen that this ratio is initially small, but rises to a maximum at intermediate times. It is also systematically larger for smaller values of l_0 – at $l_0/\eta = 1/4$, the peak value is about 2.0, which illustrates the importance of considering second moments in addition to the first. The large-time limit for this ratio can be understood by invoking the asymptotic form of the separation p.d.f., i.e. (Yeung 1994)

$$P(l,t) = \frac{1}{\sigma}\sqrt{\frac{2}{\pi}}\left(\frac{l}{\sigma}\right)^2 \exp\left(-\frac{1}{2}\frac{l^2}{\sigma^2}\right), \tag{12}$$

where $\sigma^2(t)$ is the variance of each Cartesian component of the separation vector. This p.d.f. has as its nth order moment

$$\langle l^n \rangle = \frac{\sigma^n}{\sqrt{\pi}} 2^{n/2+1} \Gamma\left(\frac{n}{2} + \frac{3}{2}\right), \tag{13}$$

where $\Gamma(.)$ is the gamma function. Taking $n = 1$ and $n = 2$ in turn gives $\sigma_l/\langle l \rangle = 0.422$ which is closely approached at large times in figure 7. Furthermore, substitution into (11) gives the ratio 1.085 for $\langle l^2 \rangle^{1/2}/\langle l \rangle$ which is also consistent with the quantities in figures 5 and 6 becoming nearly (but not exactly) the same at large times.

The third moment of the separation distance is of greatest interest in the search for inertial range scaling. It is well known that Richardson (1926) suggested the behaviour

$$\langle l^2 \rangle = g \langle \epsilon \rangle t^3 \tag{14}$$

under the conditions (i) $\eta \ll l_0 \ll L_1$, (ii) $\tau_\eta \ll t \ll T_L$ and (iii) $l \gg l_0$ (such that the details in initial conditions cease to be important). However, unambiguous

observations of this scaling are elusive, and estimates of the Richardson constant have varied widely, from 0.06 to 3.5 (Sawford 2001). In principle, if (14) does hold, then a plot of $\langle l^2\rangle^{1/3}$ versus t on linear scales should reveal a linear segment of slope $(g\langle\epsilon\rangle)^{1/3}$ passing through the origin. Ishihara & Kaneda (2002) have applied this approach to data at slightly higher Reynolds number ($R_\lambda = 283$) and suggested $g \approx 0.7$.

In figure 8, we show plots of $\langle l^2\rangle^{1/3}$ versus t normalized by Kolmogorov variables. Figure 8(*b*) a blow-up of the data within the range $t/\tau_\eta \leqslant 16$. The plotting format here is similar to figure 1 of Ishihara & Kaneda (2002) which showed un-normalized data, with circles on each line marking the time scale $\tau_0 = (l_0^2/\langle\epsilon\rangle)^{1/3}$ associated with each l_0. In agreement with these previous authors, we find some approximate linear behaviour in $\langle l^2\rangle^{1/3}$, but a close inspection of figure 8 shows that these linear portions have a definite non-zero intercept if extrapolated backwards towards $t = 0$. Of the six values of l_0 available, the case $l_0/\eta = 16$ is perhaps closest to inertial-range conditions. If the non-zero intercept is ignored, then the linear portion of the $l_0/\eta = 16$ curve gives $g = (0.94)^3 = 0.83$. However, it must be noted that in the present data $\tau_0/\tau_\eta \approx 6.5$ whereas T_L/τ_η is only about 20, so that conditions (i) and (iii) cited in the preceding paragraph cannot be satisfied simultaneously. Furthermore, it is accepted that (e.g. Yeung 2002) Kolmogorov similarity for single-particle Lagrangian statistics requires higher Reynolds numbers, and there seems as being no reason to expect that the Reynolds-number requirements for inertial scaling in two-particle statistics would be any less stringent. Consequently, we believe that, while it may be safe to regard g as being of order unity, claims of precise determination of g in DNS of currently available or slightly higher Reynolds number must be treated with caution. In Part 2, further remarks are made on this issue, in part from a modelling perspective.

In the application of dispersion models to the prediction of concentration variance, the key quantity is the separation p.d.f. (Batchelor 1952; Thomson 1990), also known as the distance-neighbour function (Richardson 1926). In figure 9, we show the p.d.f. of the normalized separation distance $l/\langle l\rangle$ at different times, for small initial separation at $l_0/\eta = 1/4$. An inset on semi-log scaling is also provided to highlight the behaviour at values of l much larger than the mean. At $t = 0$ (not shown), this p.d.f. is (for any choice of l_0) a delta-function at unity. Subsequently, in figure 9, we can see a rapid change in shape, with the p.d.f. stretching out with a long tail at intermediate times, indicating that some particle pairs have drifted far apart. This feature is most pronounced for line *C* in the figure, which reaches to more than 30 $\langle l\rangle$ and is also (see figure 7) in the time range where the $\sigma_l/\langle l\rangle$ ratio is the largest. At later times (lines *D*, *E*), the p.d.f. relaxes back towards more moderate values of the normalized separation, in part owing to an increase of $\langle l\rangle$ and a gradual trend towards the Gaussian limit for separation vectors.

The extent and shape of the p.d.f. of $l/\langle l\rangle$ as noted above is quite different for the case of large l_0, which is shown in figure 10 for $l_0/\eta = 256$ at the same Reynolds number. In this case, nearly all samples in the p.d.f. lie within the range $[0, 3\langle l\rangle]$ at all times. The p.d.f. is also seen to stretch out more evenly for values of l less than and greater than $\langle l\rangle$, which implies that, at small times, some particle pairs drift back towards each other. Whereas, at later times, the p.d.f. does retain some positive skewness (line *E*), the likelihood of l much larger than the mean is evidently much less than in the case of small initial separations.

To characterize the shape of the separation p.d.f. quantitatively we show the evolution of skewness and flatness factors of l in figures 11 and 12. The most prominent features are the high skewness and flatness for small initial separations

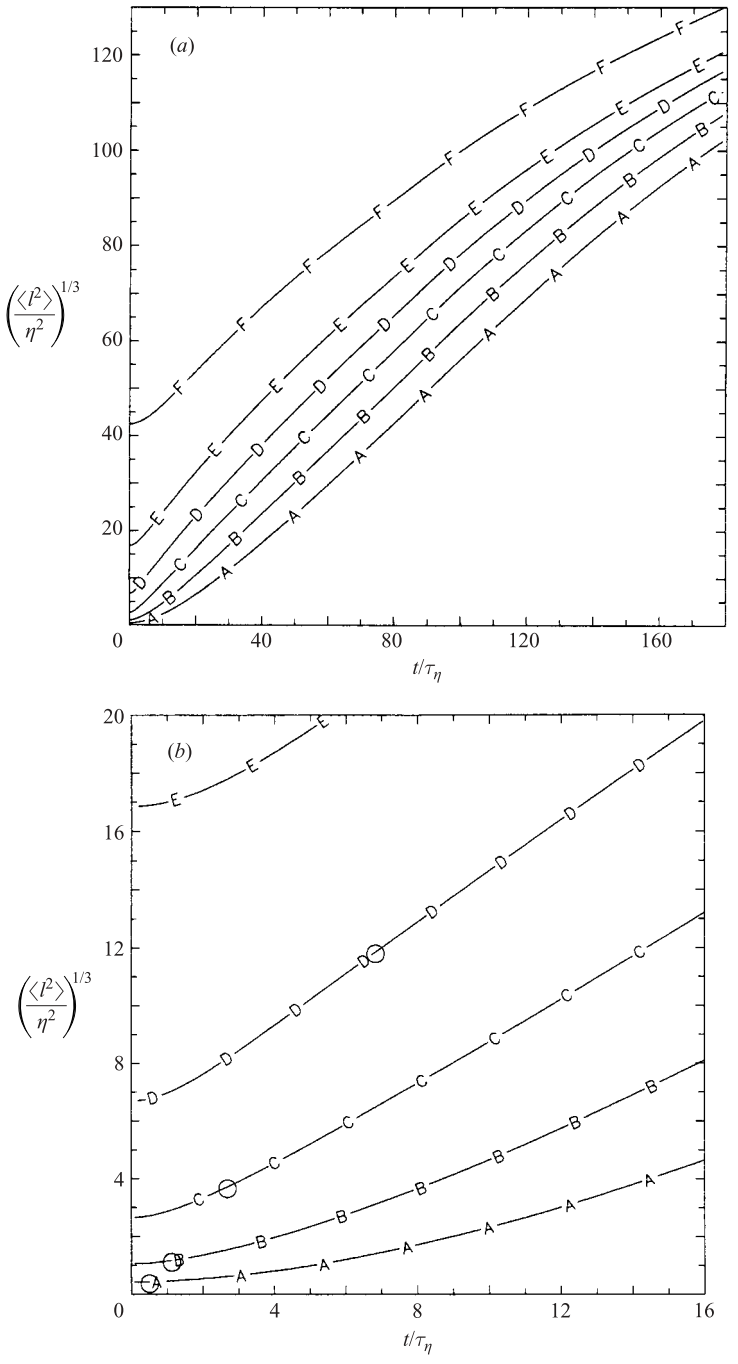

FIGURE 8. (*a*) Evolution of 1/3 power of mean-squared separation at $R_\lambda = 230$, with $l_0/\eta = 1/4$, 1, 4, 16, 64 and 256. (*b*) Same as (*a*), but for the first 16 τ_η in time only. Circles on each curve marks the time scale $\tau_0 = (l_0^2/\langle\epsilon\rangle)^{1/3}$ corresponding to a given l_0.

and intermediate times (on a logarithmic scale): for $l_0/\eta = 1/4$ the peak levels of skewness and flatness occurring at $t/\tau_\eta \approx 6$ are seen to be about 11 and of order 300, respectively. Clearly, this indicates that particle-pair dispersion is a highly intermittent

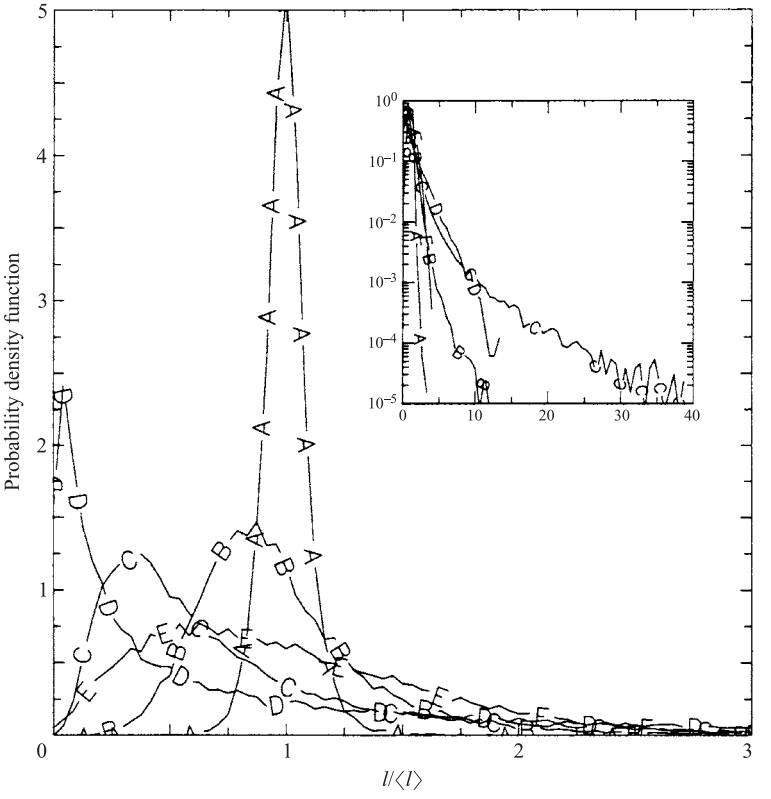

FIGURE 9. Probability density function of normalized separation distance $l/\langle l \rangle$ from 512^3 DNS, for $l_0/\eta = 1/4$. Data taken at (lines A–E) normalized times $t/\tau_\eta = 1/2$, 2, 8, 32 and 128. Inset shows the same data on semi-log scales, with wider bins extended to capture larger samples.

process, where (as noted in Yeung 1994) a given pair of particles may suddenly move far apart in relatively short time intervals. In fact, as noted in § 2, such high levels of intermittency have necessitated the use of more particle-pair samples in simulations at higher Reynolds number. In our data, this requirement was met by repeating an earlier part of the simulation with eight times as many samples for the three smallest initial separations. The resulting discontinuity in sample size is reflected by small kinks in lines *A*–*C* at $t/\tau_\eta = 20$, which are small enough for results at later times to be considered statistically robust.

Both the small- and large-time limits in figures 11 and 12 are amenable to theoretical explanation. Because all particle pairs for a given l_0 have the same separation at $t = 0$, deviations from the mean at small times are entirely due to the properties of u_r. Furthermore, since at small times most particle pairs have nearly the same separation, u_r essentially behaves as an Eulerian longitudinal velocity difference (at separation l_0), which is negatively skewed and non-Gaussian except in the limit of infinitely large-scale separation. The initial values of the observed skewness are indeed negative, whereas the initial flatness factor decreases monotonically with l_0 towards the Gaussian value of 3. The near-coincidence of lines *A* and *B* at early times is consistent with u_r becoming proportional to the longitudinal velocity gradient (such as $\partial u/\partial x$) of skewness about -0.5 as l_0 is reduced below η. It may also be noted that the skewness of l quickly becomes positive for small l_0, suggesting that some

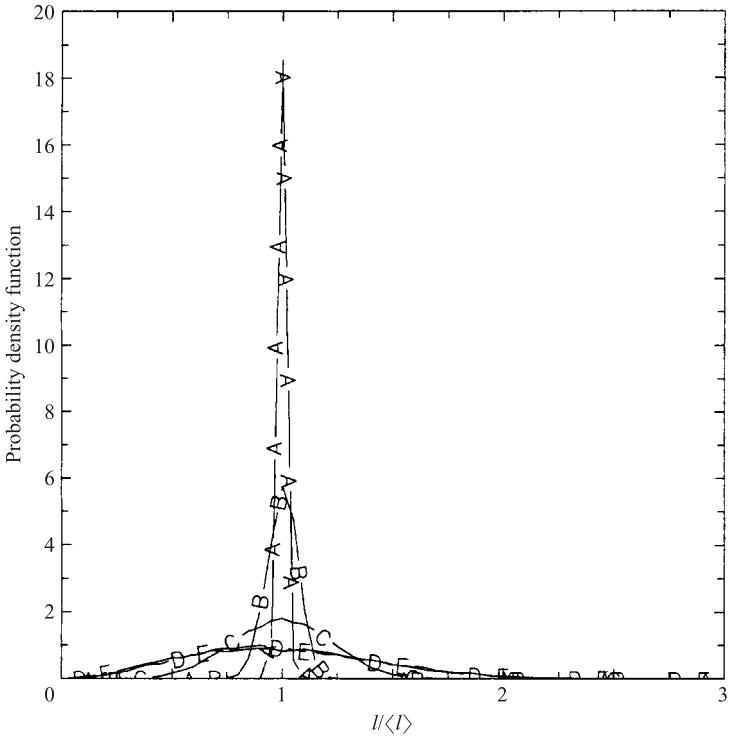

FIGURE 10. Same as figure 9, but for $l_0/\eta = 256$.

particle pairs begin to break away from each other. This effect is much weaker for large l_0, where the p.d.f. changes slowly and the skewness remains negative for several Kolmogorov time scales.

At sufficiently large times (occurring earlier for large l_0) $\boldsymbol{l}$ is expected to behave as a vector with independent and identically distributed Gaussian coordinate components. This requires that the displacement of each particle becomes Gaussian and that the particle-pair displacements become independent (or at least uncorrelated) with each other. The latter process is slow because of memory effects (Yeung 1994). In any case, the long-time asymptotic behaviour is a chi-square distribution of three degrees of freedom for l^2, such that the corresponding skewness and flatness factors of l are approximately 0.49 and 3.1. Although this value of the flatness factor is little different from Gaussian and (as in figure 12) may be somewhat obscured by sampling limitations, larger deviations from Gaussianity are likely in anisotropic flows (Shen & Yeung 1997).

A general effect of increasing Reynolds number in turbulence is stronger intermittency at the small scales. In figure 13, we illustrate this for relative dispersion in terms of the skewness of the separation distance, by showing data at the lowest and highest Reynolds number (and at two values of l_0/η). It can be seen that, at given l_0/η and t/τ_η, intermittency as measured by the skewness does become more intense with increasing Reynolds number, with the peak skewness occurring earlier in time. Reference to data in figure 6 (and corresponding data at lower Reynolds number) shows that for $l_0/\eta = 1/4$, at the time of peak skewness, $\langle l \rangle/\eta$ is about 0.9 for both R_λ 38 and 230. On the other hand, the distribution of separation distances at intermediate times spans a very wide range of scales – which is wider yet at

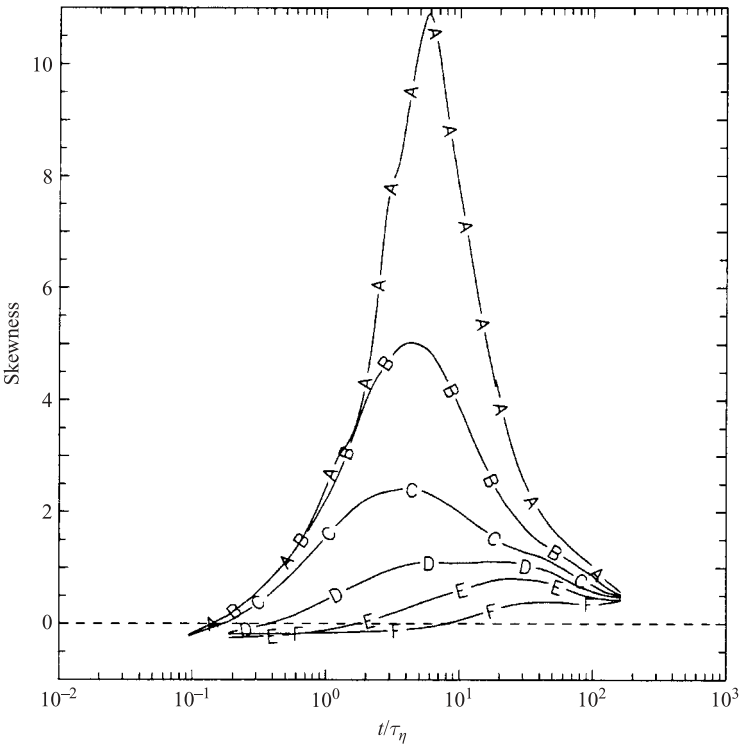

FIGURE 11. Evolution of skewness (μ_3) of separation distance (l) from 512^3 DNS, for (lines A–F) $l_0/\eta = 1/4$, 1, 4, 16, 64 and 256. Dashed line marks Gaussian value of 0.

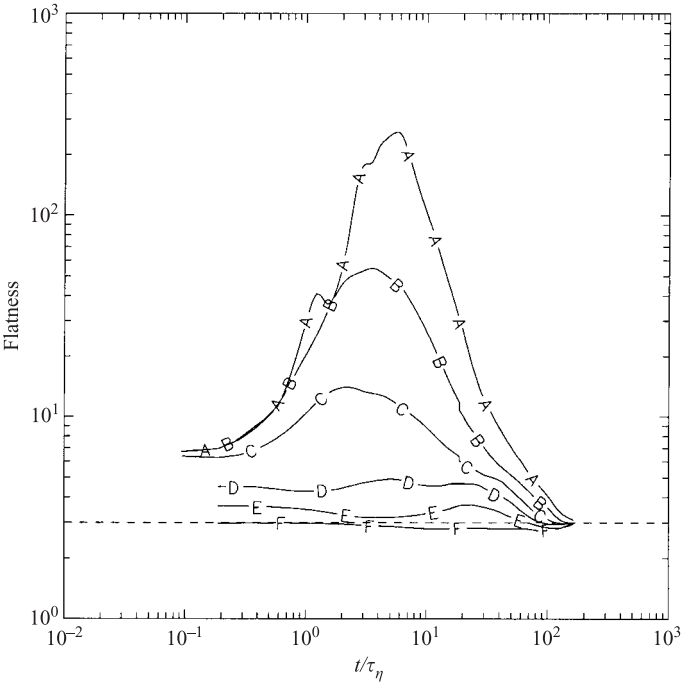

FIGURE 12. Same as figure 11, but for the flatness factor (μ_4). Dashed line marks Gaussian value of 3.

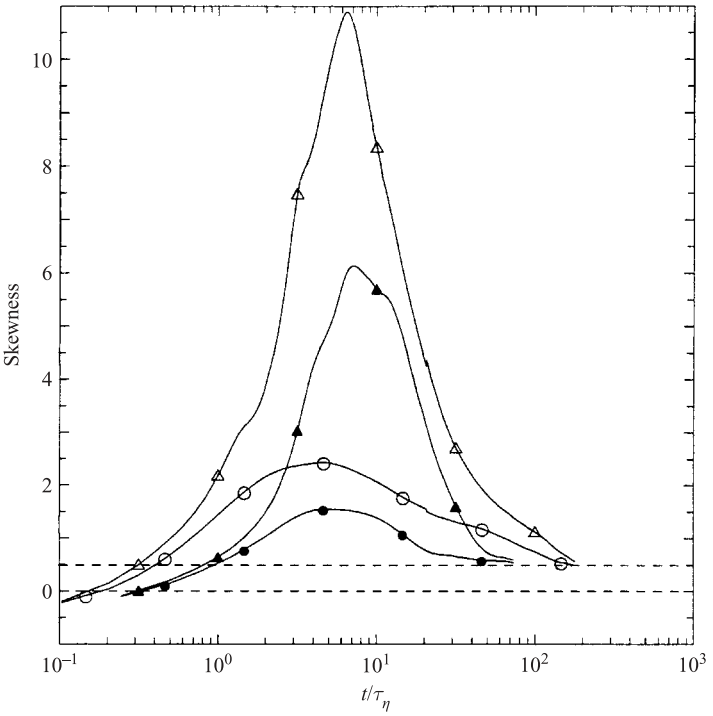

FIGURE 13. Reynolds-number effects on the skewness of the separation distance at different Reynolds numbers and initial separations. Triangles for $l_0/\eta = 1/4$, circles for $l_0/\eta = 4$; open symbols for $R_\lambda = 230$, closed symbols for $R_\lambda = 38$.

higher Reynolds number. In addition, it can be seen that (as in the discussion of figure 5), because the approach to large-time behaviour scales with T_L, on a time axis normalized by τ_η it takes longer for the higher-Reynolds-number data to reach the large-time limit.

It may be mentioned here that one possible approach for the modelling of mean-square dispersion is to write it in terms of a two-time covariance of the relative velocity ($\boldsymbol{u}^{(r)}$) (which was modelled in Ishihara & Kaneda 2002), as

$$\langle \Delta l_i \Delta l_i \rangle(t) = \int_0^t \int_0^t \left\langle u_i^{(r)}(t') u_i^{(r)}(t'') \right\rangle \, \mathrm{d}t' \, \mathrm{d}t''. \tag{15}$$

In isotropic turbulence, this covariance can be expanded as

$$\left\langle u_i^{(r)}(t') u_i^{(r)}(t'') \right\rangle = 2\langle u_i u_i \rangle [\rho_L(t', t'') - \rho_{2L}(t', t'')], \tag{16}$$

where ρ_L and ρ_{2L} are, respectively, one- and two-particle Lagrangian velocity correlations. In particular, ρ_{2L} is the correlation coefficient between the velocities of two different particles (separated in space) recorded at different times. The behaviour of ρ_{2L} is (Sawford 1982; Yeung 1997*b*) dominated by effects of time lag rather than particle-pair separation. However, only heuristic phenomenological models are available, which furthermore can only provide second-moment information.

4.2. *Separation speed and vector alignments*

More detailed understanding of the evolution of the separation distance can be obtained by studying the separation speed, u_r, which in quasi-one-dimensional models

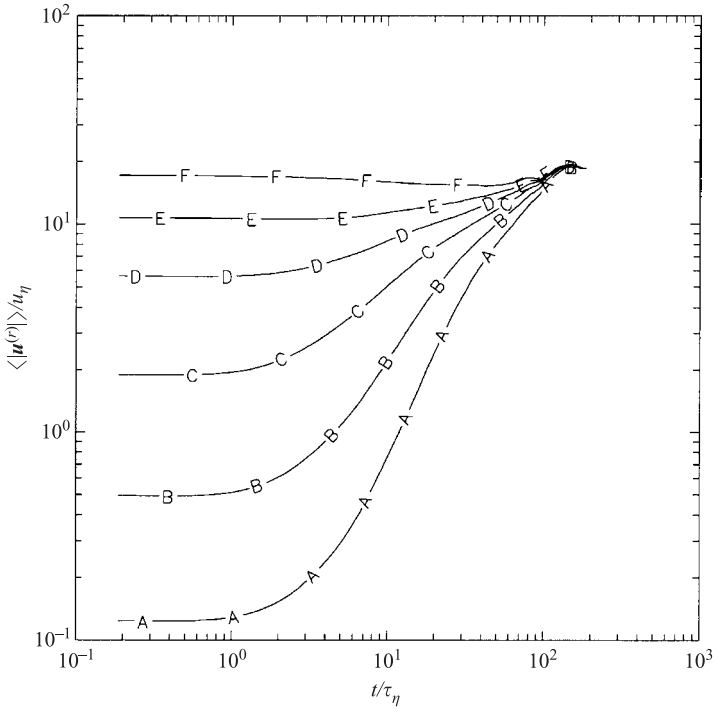

FIGURE 14. Mean value of relative velocity magnitude, with symbols same as in figure 5.

is integrated in time to give the separation distance itself. As per the definition in (1), the behaviour of u_r is sensitive to the angular alignment between the separation ($\boldsymbol{l}$) and relative velocity ($\boldsymbol{u}^{(r)}$) vectors.

We emphasize that u_r is the component of $\boldsymbol{u}^{(r)}$ along the direction of $\boldsymbol{l}$, and should not be confused with the magnitude of $\boldsymbol{u}^{(r)}$ itself. However, to provide a contrast, the mean of the relative velocity magnitude, i.e. $\langle|\boldsymbol{u}^{(r)}|\rangle$, is shown first in figure 14, normalized by the Kolmogorov velocity scale (u_η, $\equiv[\nu\langle\epsilon\rangle]^{1/4}$). Being sensitive mainly to the distribution of separation distances, this quantity is seen to generally increase with the initial separation. For the case of large l_0 (line F) the curve decreases within an intermediate time period as (see figure 10) some of the particle pairs move back towards each other. At large times, it is clear that data for all l_0 converge upon the same asymptotic limit, which can be derived analytically by assuming that particle pair velocities become independent of each other (whereupon each coordinate component of $\boldsymbol{u}^{(r)}$ has variance equal to twice of the single-point velocity variance). In isotropic turbulence this also implies that $|\boldsymbol{u}^{(r)}|$ behaves as the square root of the sum of the squares of three independent Gaussian random variables, with a p.d.f. of the same form as (12). Use of (13) then gives $\langle|\boldsymbol{u}^{(r)}|\rangle = 1.63[\langle {u_1^{(r)}}^2\rangle]^{1/2}$, which together with the isotropy relation $\langle\epsilon\rangle = 15\nu u'^2/\lambda^2$ then leads to

$$\frac{\langle|\boldsymbol{u}^{(r)}|\rangle}{u_\eta} = \frac{1.63\sqrt{2}}{(15)^{1/4}} R_\lambda{}^{1/2} = 1.17 R_\lambda{}^{1/2}, \tag{17}$$

depending on Reynolds number alone. At $R_\lambda = 230$ for the 512^3 simulation, this relation gives $\langle|\boldsymbol{u}^{(r)}|\rangle/u_\eta \sim 17.8$, which is satisfied well by the data in figure 14.

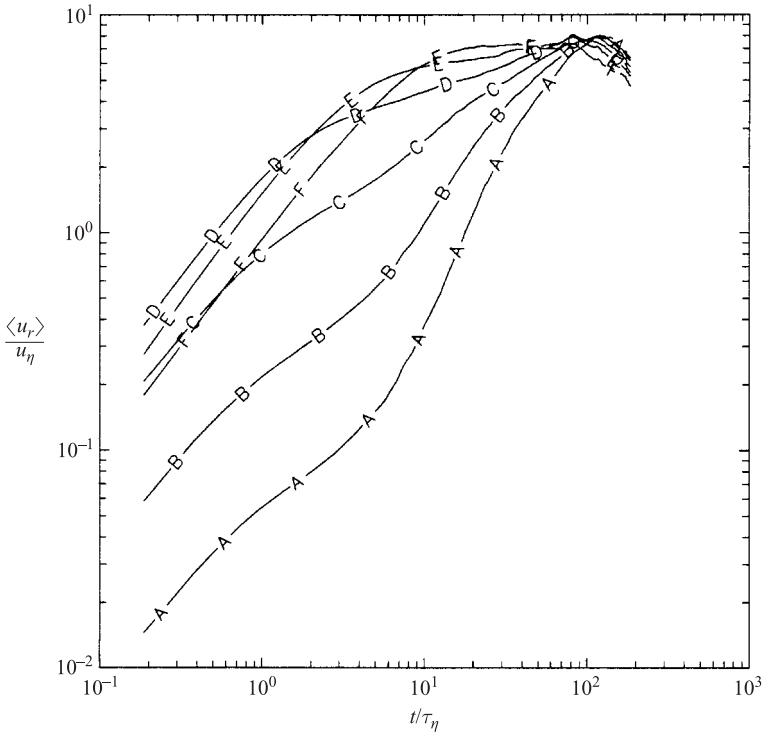

FIGURE 15. Same as figure 15, but for mean value of separation speed (u_r).

The mean of the separation speed has a different behaviour, which is shown in figure 15. This quantity is initially zero because of homogeneity in the Eulerian velocity field, but the monotonic increase of the mean separation distance with time implies that at any time $t > 0$, u_r, has a positive mean value, which is associated with the probability of acute-angled alignment between $\boldsymbol{l}(t)$ and $\boldsymbol{u}^{(r)}(t)$ being greater than 0.5 (Yeung 1994). The dependence on both initial separation and time seen in this figure is more complex than that for the relative velocity magnitude in figure 14. In particular, at early and intermediate times, $\langle u_r \rangle$ has a non-monotonic dependence on l_0, whereas, at large times, $\langle u_r \rangle$ decays systematically with particle pairs of smallest l_0 having the largest $\langle u_r \rangle$. Both of these features are a result of changing angular alignment between $\boldsymbol{l}$ and $\boldsymbol{u}^{(r)}$, which we discuss later in this section.

To help understand the origins of the intermittency of separation distance (seen in figures 11 and 12), and to provide a reference for future model comparisons, we show the skewness and flatness factors for u_r in figures 16 and 17. As already noted in the discussion of figures 11 and 12, at small times, the behaviour is similar to that of the Eulerian spatial difference over a distance l_0. Indeed, data at $t = 0$ (not shown in the plots because of log scales) give the skewness for both $l_0/\eta = 1/4$ and 1 as equal to -0.55, which is close to that usually observed for longitudinal velocity gradients in isotropic turbulence at moderate-to-high Reynolds numbers. Peak intermittency levels for u_r are seen to be higher than those of l, and also occur at slightly earlier times. This suggests that intermittency in u_r can be regarded as the cause of intermittency in l, with the time delay being associated with memory effects implied by the relation $l(t) = l_0 + \int_0^t u_r(t')\,\mathrm{d}t'$. However, there is a characteristic difference between the statistics of u_r and l at large times, when u_r is seen to become

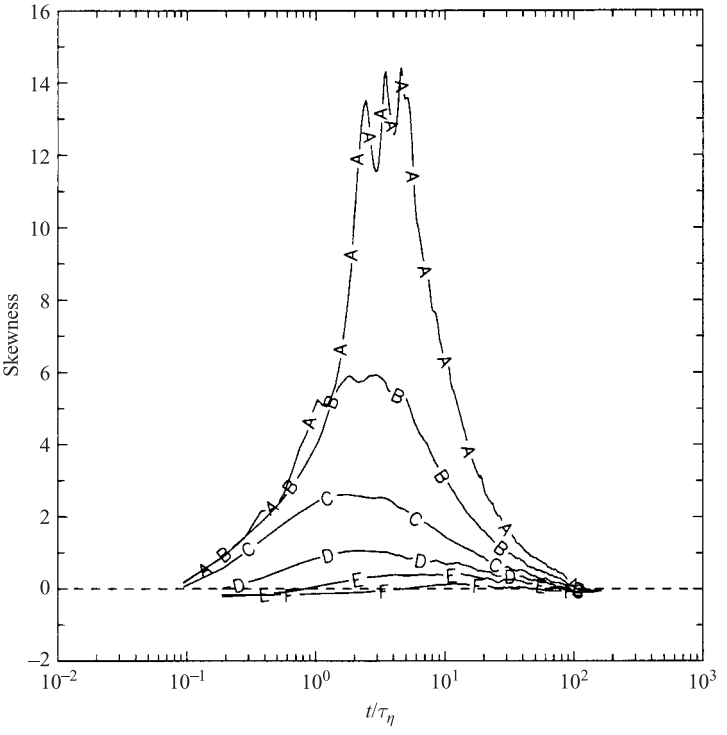

FIGURE 16. Same as figure 11, but for skewness of the separation speed (u_r).

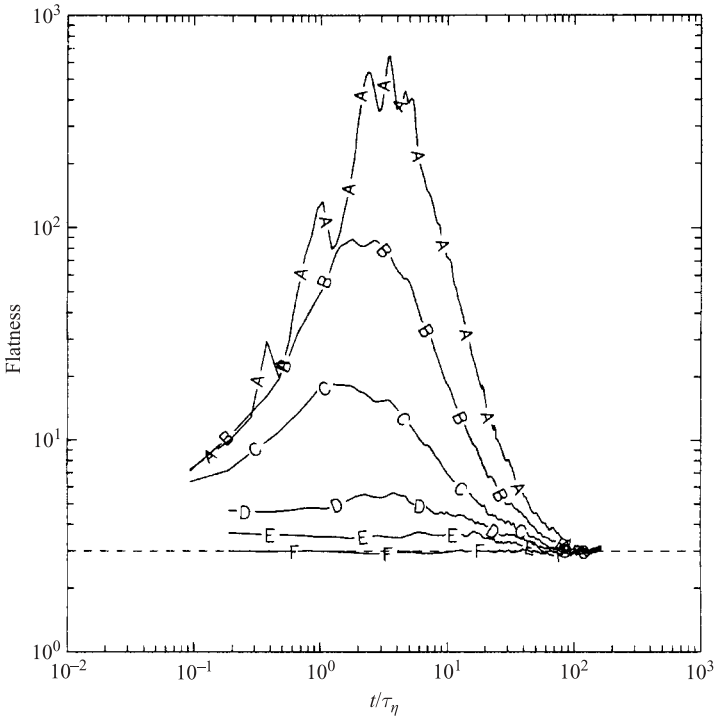

FIGURE 17. Same as figure 16, but for the flatness factor.

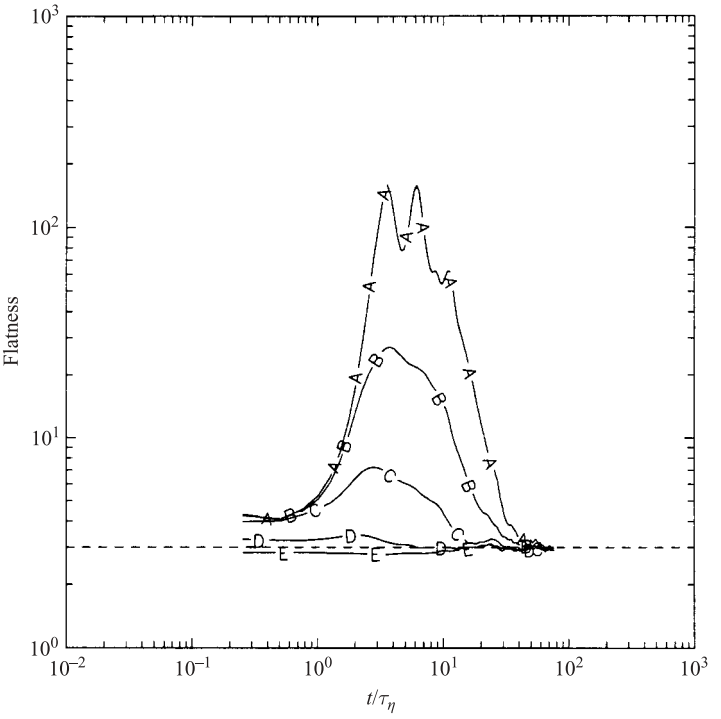

FIGURE 18. Same as figure 17, but for data at $R_\lambda = 38$, with $l_0/\eta = 1/4$, 1, 4, 16 and 64.

Gaussian. This property is a result of the Gaussianity of the single point velocity, together with neutral alignment between $\boldsymbol{l}$ and $\boldsymbol{u}^{(r)}$ for particles far apart, such that u_r ultimately behaves as the difference between two independent Gaussian variables.

Reynolds-number effects on the statistics of u_r are illustrated by comparing flatness values with data at lower Reynolds number in figure 18. The intermittency levels are, as expected, reduced at lower Reynolds number, with the flatness at early times for small l_0 being consistent with known Reynolds number trends (e.g. Sreenivasan & Antonia 1997) for the flatness of velocity gradients in turbulence. Nevertheless, for small l_0, the separation velocity p.d.f. can still become very intermittent at intermediate times, with peak flatness in the case of $l_0/\eta = 1/4$ being of the order 100 in figure 18.

It should be noted that the flatness of u_r shown in figures 17 and 18 is different from that of a coordinate component of the relative velocity (denoted as $u_i^{(r)}$), which was reported earlier by Yeung (1994) and used for comparisons by Heppe (1998) and Malik & Vassilicos (1999). Because three distinct choices of the orientation of $\boldsymbol{l}(0)$ are used, at early times the distribution of $u_i^{(r)}$ consists of mixed samples of longitudinal and (unskewed) transverse velocity differences. The physical meaning of the statistics of $u_i^{(r)}$ is thus not as clear as that of u_r considered in this paper. On the other hand, because both the separation vector and the relative velocity gradually become randomly oriented with respect to fixed coordinate axes, at later times, the statistics u_r and $u_i^{(r)}$ are nearly the same.

To further analyse the differences between relative velocity and separation speed, it is helpful to note that $\boldsymbol{u}^{(r)}(t)$ evolves by both a change in magnitude due to motion along $\boldsymbol{l}$ and a change in direction due to motion in the plane orthogonal to $\boldsymbol{l}$. Consequently, we distinguish between projections of the relative velocity along $\boldsymbol{l}$, which is given by u_r (as defined in (1)), and that perpendicular to $\boldsymbol{l}$, which is given

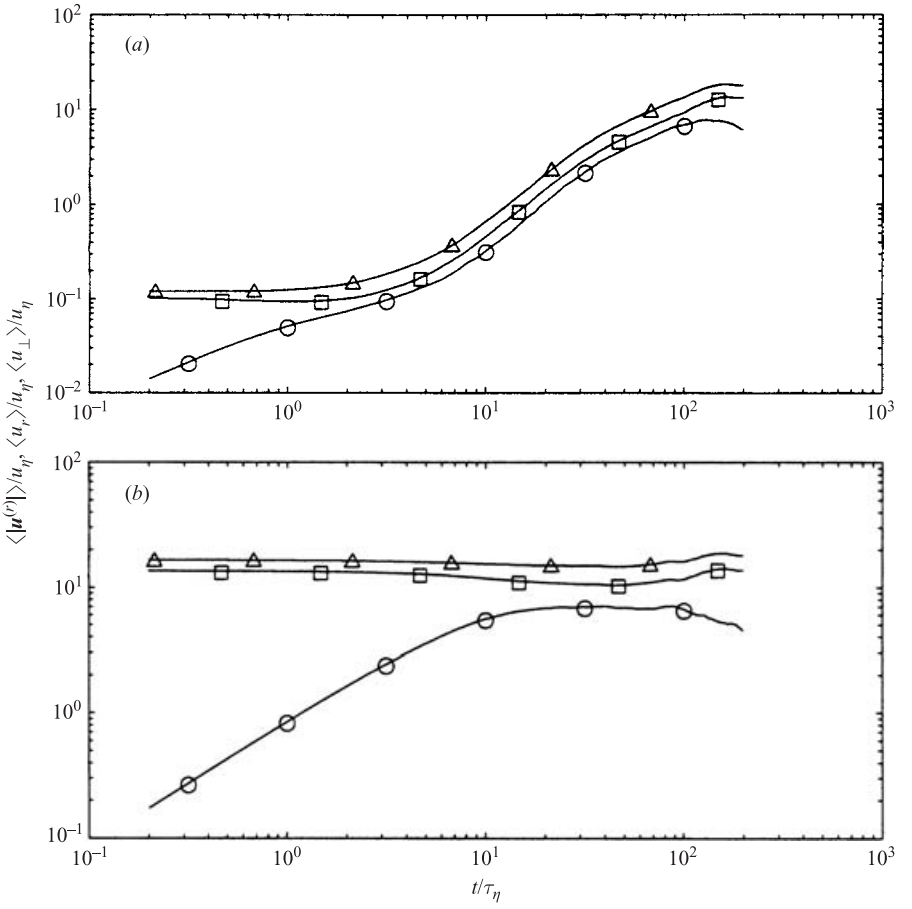

FIGURE 19. Evolution of $\langle|\boldsymbol{u}^{(r)}|\rangle$ (△), $\langle u_r\rangle$(○) and $\langle u_\perp\rangle$ (□), normalized by Kolmogorov scales of time and velocity (τ_η, u_η), for data at $R_\lambda = 230$: for (*a*) $l_0/\eta = 1/4$ and (*b*) $l_0/\eta = 256$.

by

$$u_\perp \equiv \left|\boldsymbol{u}^{(r)}\right| |\sin\theta_1| \tag{18}$$

(with θ_1 being the angle between $\boldsymbol{u}^{(r)}$ and $\boldsymbol{l}$). Whereas the 'longitudinal' velocity u_r determines the rate of change of the separation distance, the 'transverse' component $u_\perp$ (which is by definition always positive) is responsible for changes in the angular orientation of the separation vector.

Figure 19 gives a comparison of the mean values of $|\boldsymbol{u}^{(r)}|$, u_r and $u_\perp$, for both small and large initial separations. It can be seen that $u_\perp$ has a larger mean value than u_r and follows closely the behaviour of $|\boldsymbol{u}^{(r)}|$ at all times. The ratio between the mean values of $\langle u_r\rangle$ and $\langle u_\perp\rangle$ is especially large at early times for particle pairs with large l_0, which shows that it takes a relatively long period of time for significant alignment between $\boldsymbol{u}^{(r)}$ and $\boldsymbol{l}$ to develop. For small l_0, we observe sustained growth in all three quantities shown, corresponding to larger relative velocities as l increases rapidly compared with its initial value. At later times (i.e. $t \gg T_L$), the vectors $\boldsymbol{u}^{(r)}$ and $\boldsymbol{l}$ become less closely aligned, which causes $\langle u_r\rangle$ to decrease slowly (while remaining positive). In addition, as noted before, as the particles become far apart the coordinate components of $\boldsymbol{u}^{(r)}$ behave increasingly as independent and Gaussian. Accordingly,

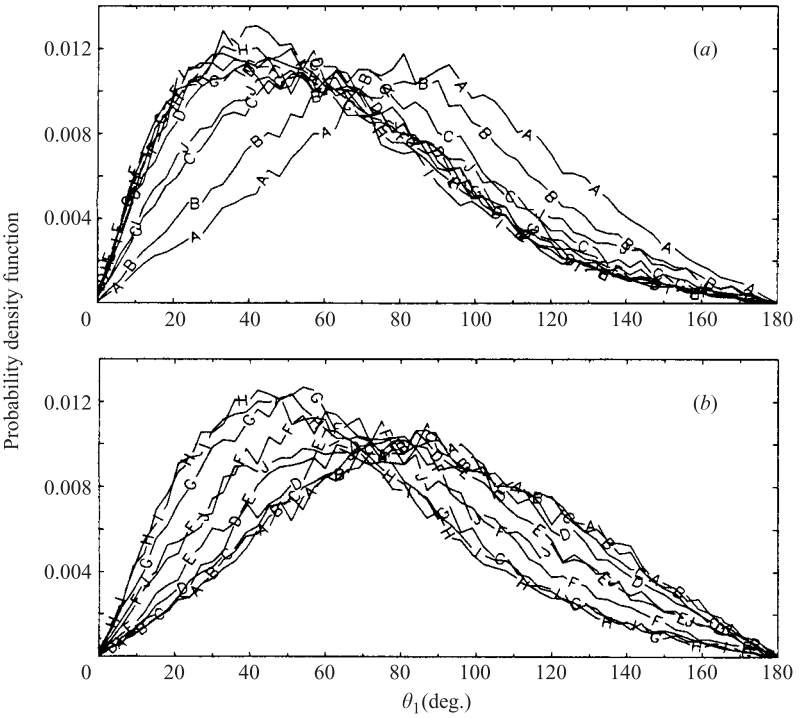

FIGURE 20. Probability density function of θ_1 (in degrees) at $t/\tau_\eta = 0$, 0.4, 1, 2, 4, 8, 16, 32, 64 and 128 (lines A–J), for data at $R_\lambda = 230$: (*a*) $l_0/\eta = 1/4$ and (*b*) $l_0/\eta = 256$.

the statistics of $|\boldsymbol{u}^{(r)}|$ and $u_\perp$ become similar to those expected for $|\boldsymbol{u}^{(r)}|^2$ and $u_\perp^2$ to be chi-square distributed with three and two degrees of freedom, respectively.

The statistical distribution of the alignment angle θ_1 is a determining factor in the statistics of u_r versus $u_\perp$ as discussed above. Figure 20 shows the p.d.f. of this angle at selected time instants for both small and large initial separations. Because particle-pair statistics at $t = 0$ are essentially Eulerian, initially there is no preferred alignment between $\boldsymbol{u}^{(r)}$ and $\boldsymbol{l}$, which implies that the p.d.f. of θ_1 is (as seen in line *A*) nearly symmetric. Subsequently, for small l_0 it is clear that the p.d.f. shifts towards increased acute alignment very quickly (in fact, in less than one τ_η). However, this trend is reversed between 10 to 20 τ_η, and the p.d.f. ultimately relaxes (line *J*) back towards a state of weaker alignment. The peak value of $\langle \cos\theta_1 \rangle$ is found to be about 0.46, with the probability of acute alignment ($0 < \theta_1 < 90^\circ$) being slightly greater than 0.8, which is close to the value observed at lower Reynolds number (Yeung 1994). The data for large l_0 (figure 20*b*) follows roughly the same trend in time, but the alignment builds up more slowly than for small l_0.

The fact that $\langle u_\perp \rangle$ is larger than $\langle u_r \rangle$ implies that there is considerable relative motion in directions perpendicular to $\boldsymbol{l}(t)$. Over time, this effect tends to change the orientation of $\boldsymbol{l}(t)$ and thus would influence the directional dependence of dispersion. For isotropic turbulence, the vector $\boldsymbol{l}(t)$ is ultimately expected to become randomly oriented in space regardless of its initial orientation. However, it is of interest to compare mean-squared separation in the direction of $\boldsymbol{l}(0)$, i.e.

$$\langle s^2 \rangle \equiv \left\langle (\boldsymbol{l}(t) \cdot \boldsymbol{l}(0))^2 / l_0^2 \right\rangle = \langle l^2 \cos^2 \theta_2 \rangle, \tag{19}$$

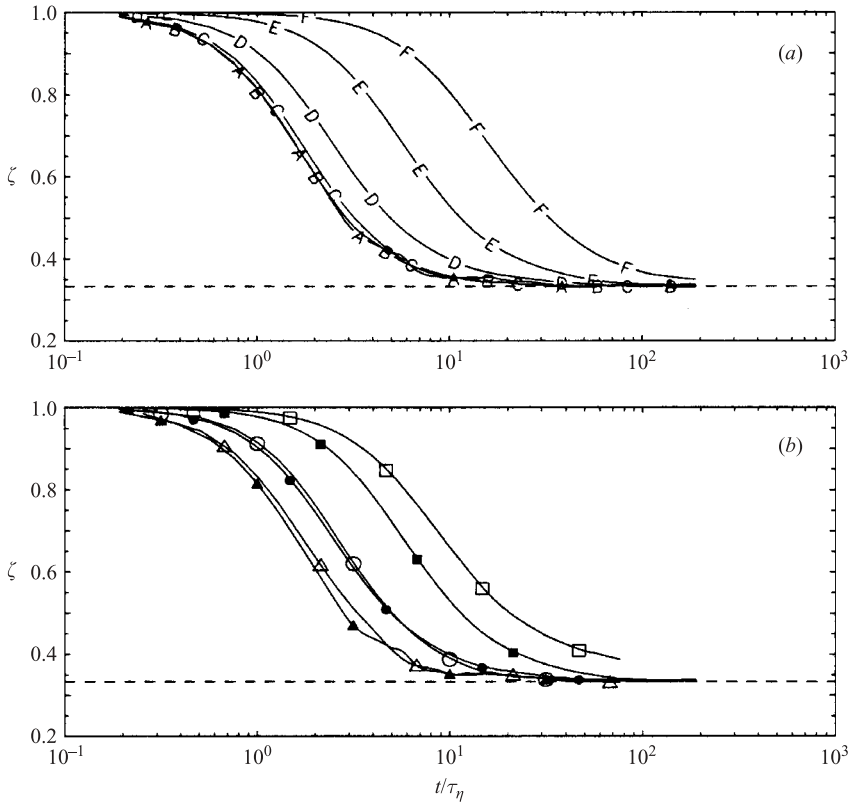

FIGURE 21. Evolution of the ratio $\zeta = \langle s^2 \rangle / \langle l^2 \rangle$: (*a*) $l_0/\eta = 1/4$, 1, 4, 16, 64 and 256 (A–F) at $R_\lambda = 230$; (*b*) $l_0/\eta = 1/4$, 16, 64 (△, ○, □) at $R_\lambda = 38$, compared with $l_0/\eta = 1/4$, 16, 64 (corresponding solid symbols) at $R_\lambda = 230$.

(with $\theta_2(t)$ as defined in § 1), with $\langle l^2 \rangle$ itself. Figure 21 shows the evolution of the ratio $\zeta = \langle s^2 \rangle / \langle l^2 \rangle$ for both small and large initial separations, and at the lowest and highest Reynolds numbers in the simulations. Clearly, as expected, this ratio decreases from unity at $t = 0$ towards the value $1/3$ at large times. The time taken to reach this asymptote depends on l_0, since if $\boldsymbol{l}$ is initially a long vector then it would take a longer period of time for its orientation to change significantly. Nevertheless, there is a remarkable similarity in shape between the curves for small and large l_0, with ζ showing an intermediate period of logarithmic decrease in both cases.

The p.d.f. of θ_2 concerned with the angular orientation of $\boldsymbol{l}$ is shown in figure 22. The key issues are how quickly this p.d.f. evolves towards the shape for neutral alignment, and whether (as in Yeung & Borgas 1998) its functional form at intermediate times can be modelled accurately. Comparison with figure 21 shows that most of the transition occurs at times when ζ has decreased to nearly $1/3$: for instance for $l_0/\eta = 1/4$, although by time $t/\tau_\eta = 2$, we find that ζ has dropped to 0.6, the probability of θ_2 being acute (line *D* in the figure) then is still almost 1.0. For small l_0, the p.d.f. at later times effectively coincides with the theoretical asymptote (dashed curve) which corresponds to $\cos\theta_2$ having a uniform distribution between -1 and 1. By contrast, as stated earlier, the alignment for large l_0 changes rather slowly, with the p.d.f. being still asymmetric and evolving at the end of the simulations.

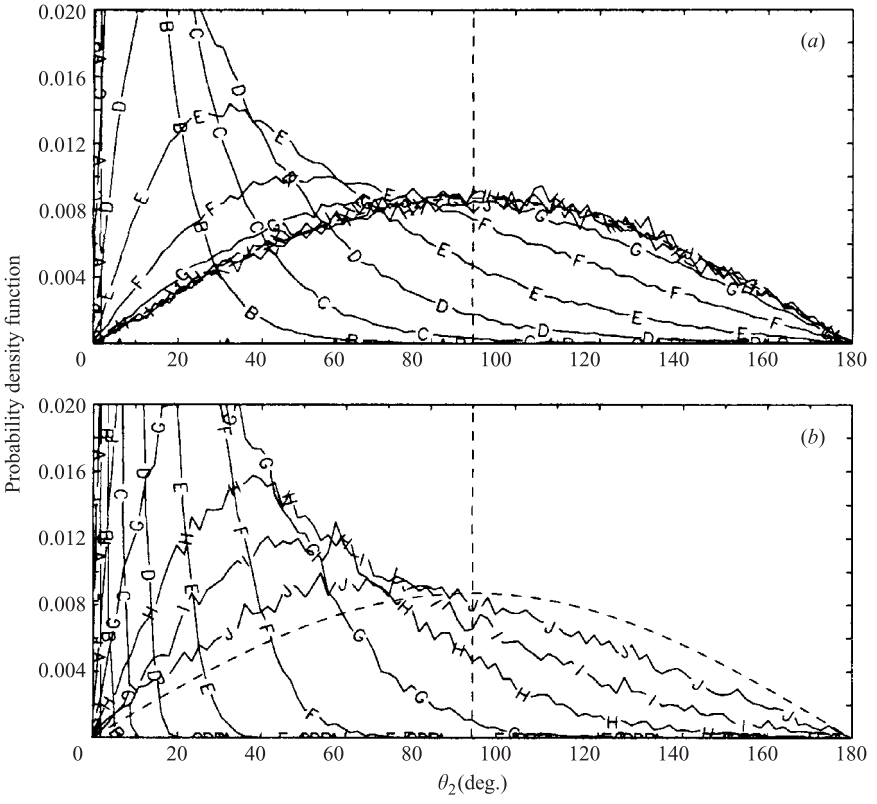

FIGURE 22. Probability density function of θ_2 at different times, corresponding to data in figure 20. Note that some of the high peaks near $\theta_2 = 0$ for early times are truncated. The dashed curve represents the case of purely random orientation.

5. Conclusions and discussion

In this paper, we have presented a detailed study of the Lagrangian statistics of particle-pair relative dispersion, using direct numerical simulations reaching Reynolds numbers higher than previously attained. The emphasis is on capturing the crucial dynamics, including Reynolds-number dependence, in a manner useful for developments in stochastic modelling (Part 2). The background turbulence is statistically isotropic and stationary by virtue of stochastic forcing applied at the large scales. The Taylor-scale Reynolds numbers are between 90 and 230, with the latter being (see Yeung & Zhou 1997) sufficiently high for a limited range in the Eulerian energy spectrum in wavenumber space (although not for Lagrangian quantities). The initial separation (l_0) is varied from shorter than one Kolmogorov length scale to longer than one longitudinal integral length scale in the flow.

Because of isotropy in the simulated flow, and because of interest in the development of quasi-one-dimensional models, we have focused on describing the statistical properties of the separation distance (l) and the separation speed (u_r, $\equiv \mathrm{d}l/\mathrm{d}t$) which is the relative velocity projected in the direction of the separation vector. Statistics reported include first four moments and probability density functions of l and u_r evolving in time as the particle pairs move apart on average. Results at small times are, with the proviso of adequate sampling, consistent with the Eulerian structure of the flow, whereby initially u_r behaves as a longitudinal velocity increment between

two points in space at distance l_0 apart. Similarly, at large times the dispersion results are consistent with one-particle Lagrangian statistics via the expectation that particles far apart move independently of each other.

The intermediate time regime characterized by highly non-Gaussian and intermittent behaviour for particle pairs of small initial separation poses a substantial challenge for modelling. While this non-Gaussianity is known from earlier papers (see, e.g. Durbin 1980; Sawford 1983), DNS provides the best means to directly quantify this behaviour, specifically in terms of skewness and flatness factors of both l (figures 11 and 12) and u_r (figures 16 and 17). We find that peak intermittency occurs at a time of several Kolmogorov time scales, which is arguably still in the dissipation subrange where viscous retardation of the separation process has significant effects. At the same time, the particle-pair separation p.d.f. shows that some fluid particle pairs are drifting far apart while the majority are still relatively close together. This intermittency is, as expected, stronger at higher Reynolds number.

To allow model testing with confidence, we have taken steps to address and resolve several sources of uncertainties in the DNS results. In particular, the strong non-Gaussianity and intermittency noted above leads to a requirement for a larger particle-pair ensemble at higher Reynolds number. We have quantified sampling errors via statistical confidence intervals and have ensured reliable results for skewnesses and flatnesses by using more particle pairs (close to 200 000) for up to the first 20 Kolmogorov time scales. We also note the effect of stochastic forcing in DNS in substantial temporal variability of global statistics including the energy dissipation rate, which suggests that short-time averages should be used as normalizing parameters for similarity scaling at early or even intermediate times.

A physical limitation of the present simulations is that the Reynolds number is not yet high enough for Lagrangian statistics to exhibit Kolmogorov inertial-range similarity. In particular, the normalized one-particle Lagrangian structure function (figure 3) does not show a clear plateau that would correspond to the Lagrangian Kolmogorov constant (C_0). Nevertheless, it is encouraging that two alternative schemes of deducing C_0 (figure 4) give results in close agreement, which suggests a systematic trend towards high-Reynolds-number asymptotic behaviour in our data.

The model development described in Part 2 is focused on the separation distance, which is modelled as a 'scalar' stochastic process as opposed to the full separation vector. In general, the magnitude of the separation vector is more important than its orientation, and stochastic equations for the separation distance have the advantage of avoiding non-uniqueness difficulties in the model formulation. Nevertheless, for possible use in further model refinement (e.g. the three-dimensional model devised by Kurbanmuradov 1997) and testing, we have also studied the distinctions between relative dispersion along the direction of the separation vector (leading to change in separation distance) versus that in the orthogonal plane (leading to change in orientation). Except for very large initial separation, substantial dispersion in the orthogonal plane is found to cause the separation vector to become randomly oriented, implying that the direction of the initial separation vector becomes unimportant.

In summary, we have used DNS to study relative dispersion in greater detail and at higher Reynolds number than previously feasible, and with sufficient care so that the results can be used for model development (Part 2) with confidence. Ongoing efforts are being made to extract detailed data from simulations at yet higher Reynolds numbers on 1024^3 or finer grids. Such results and those bearing upon the motion of three- and four-particle clusters (Yeung *et al.* 2003) are to be reported separately in the future.

We gratefully acknowledge support from the National Science Foundation (NSF, Grant no. INT-9526868) and the Australian Government Department of Industry, Science and Technology (International Bilateral Exchange Program no. 95/4358) which have made our collaboration possible. The computations were performed using national resources at the Cornell Theory Center and San Diego Supercomputer Center, also supported by NSF.

REFERENCES

Batchelor, G. K. 1952 Diffusion in a field of homogeneous turbulence II. The relative motion of particles *Proc. Camb. Phil. Soc.* **48**, 345–362.

Bickel, P. J. & Doksum, K. A. 1977 *Mathematical Statistics*. Holden-Day, Oakland, CA.

Borgas, M. S. & Sawford, B. L. 1991 The small-scale structure of acceleration correlations and its role in the statistical theory of turbulent dispersion. *J. Fluid Mech.* **228**, 295–320.

Borgas, M. S. & Sawford, B. L. 1994 A family of stochastic models for two-particle dispersion in isotropic homogeneous stationary turbulence. *J. Fluid Mech.* **279**, 69–99.

Borgas, M. S. & Yeung, P. K. 1998 Conditional fluid particle accelerations in turbulence. *Theoret. Comput. Fluid Dyn.* **11**, 69–93.

Borgas, M. S. & Yeung, P. K. 2004 Relative dispersion in isotropic turbulence. Part 2. A new stochastic model with Reynolds-number dependence. *J. Fluid Mech.* **503**, 125–160.

Chertkov, M., Pumir, A. & Shraiman, B. I. 1999 Lagrangian tetrad dynamics and the phenomenology of turbulence. *Phys. Fluids* **11**, 2394–2410.

Degrazia, G. & Anfossi, D. 1998 Estimation of the Kolmogorov constant C_0 from classical statistical diffusion theory. *Atmos. Environ.* **32**, 3611–3614.

Du, S., Sawford, B. L., Wilson, J. D. & Wilson, D. J. 1995 Estimation of the Kolmogorov constant (C_0) for the Lagrangian structure function, using a second-order Lagrangian model of grid turbulence. *Phys. Fluids* **7**, 3083–3090.

Durbin, P. A. 1980 A stochastic model of two-particle dispersion and concentration fluctuations in homogeneous turbulence. *J. Fluid Mech.* **100**, 279–302.

Eswaran, V. & Pope, S. B. 1988 An examination of forcing in direct numerical simulations of turbulence. *Computers Fluids* **16**, 257–278.

Fox, R. O. & Yeung, P. K. 2003 Improved Lagrangian mixing models for passive scalars in isotropic turbulence. *Phys. Fluids* **15**, 961–985.

Frisch, U., Mazzi, A., Noullez, A. & Vergassola, M. 1999 Lagrangian method for multiple correlations in passive scalar advection. *Phys. Fluids* **11**, 2178–2186.

Fung, J. C. H., Hunt, J. C. R., Malik, N. A. & Perkins, R. J. 1992 Kinematic simulation of homogeneous turbulence by unsteady random Fourier modes. *J. Fluid Mech.* **236**, 281–318.

Fung, J. C. H. & Vassilicos, J. C. 1998 Two-particle dispersion in turbulent like flows. *Phys. Rev.* E **57**, 1677–1690.

Gat, O., Procaccia, I. & Zeitak, R. 1998 Anomalous scaling in passive scalar advection: Monte Carlo Lagrangian trajectories. *Phys. Rev. Lett.* **80**, 5536–5539.

Heinz, S. 2002 On the Kolmogorov constant in stochastic turbulence models. *Phys. Fluids* **14**, 4095–4098.

Heppe, B. M. O. 1998 Generalized Langevin equation and relative turbulent dispersion. *J. Fluid Mech.* **357**, 167–198.

Hill, R. J. 2002 Scaling of acceleration in locally isotropic turbulence. *J. Fluid Mech.* **452**, 361–370.

Ishihara, T. & Kaneda, Y. 2002 Relative diffusion of a pair of fluid particles in the inertial subrange of turbulence. *Phys. Fluids* **14**, L69–L72.

Kimura, Y. & Herring, J. R. 1996 Diffusion in stably stratified turbulence. *J. Fluid Mech.* **328**, 253–269.

Kurbanmuradov, O. A. & Sabelfeld, K. K. 1995 Stochastic Lagrangian models of relative dispersion of a pair of fluid particles in turbulent flows. *Monte Carlo Meth. Applic.* **1**, 101–136.

Kurbanmuradov, O. A. 1997 Stochastic Lagrangian models of two-particle relative turbulent dispersion in high-Reynolds number turbulence. *Monte Carlo Meth. Applic.* **3**, 37–52.

La Porta, A., Voth, G. A., Moisy, F., Bodenschatz, E. & Alexander, J. 2001 Fluid particle accelerations in fully developed turbulence. *Nature* **409**, 1017–1019.

Lien, R.-C. & D'Asaro, E. A. 2002 The Kolmogorov constant for the Lagrangian velocity spectrum and structure function. *Phys. Fluids* **14**, 4456–4459.

Malik, N. A. & Vassilicos, J. C. 1999 A Lagrangian model for turbulent dispersion with turbulent-like flow structure: comparison with direct numerical simulation for two-particle statistics. *Phys. Fluids* **11**, 1572–1580.

Monin, A. S. & Yaglom, A. M. 1975 *Statistical Fluid Mechanics*, vol. 2 (ed. J. L. Lumley), MIT Press, Cambridge, MA.

Mordant, N., Metz, P., Michele, O. & Pinton, J.-F. 2001 Measurement of Lagrangian velocity in fully developed turbulence. *Phys. Rev. Lett.* **87**, art. no. 214 501.

Ott, S. & Mann, J. 2000 An experimental investigation of the relative diffusion of particle pairs in three-dimensional turbulent flow. *J. Fluid Mech.* **422**, 207–223.

Overholt, M. R. & Pope, S. B. 1996 Direct numerical simulation of a passive scalar with imposed mean gradient in isotropic turbulence. *Phys. Fluids* **8**, 3128–3148.

Overholt, M. R. & Pope, S. B. 1998 A deterministic forcing scheme for direct numerical simulations of turbulence. *Comput. Fluids* **27**, 11–28.

Physick, W. L. & Hurley, P. J. 1994 A fast Lagrangian particle model for use with three-dimensional mesoscale models. In *Air Pollution Modelling and its Application X* (ed. S. E. Gryning & M. M. Millan), pp. 235–241. Plenum, New York.

Pope, S. B. 1994 Lagrangian p.d.f. methods for turbulent flows. *Annu. Rev. Fluid Mech.* **26**, 23–63.

Reynolds, A. M. 1998 Comments on the 'Universality of the Lagrangian velocity structure function constant (C_0) across different kinds of turbulence'. *Boundary Layer Met.* **89**, 161–170.

Richardson, L. F. 1926 Atmospheric diffusion shown on a distance-neighbour graph. *Proc. Roy. Soc. Lond.* A **110**, 709–737.

Rogallo, R. S. 1981 Numerical experiments in homogeneous turbulence. *NASA TM* 81315, NASA Ames Research Center, Moffett Field, CA.

Sawford, B. L. 1982 Comparison of some different approximations in the statistical theory of relative dispersion. *Q. J. R. Met. Soc.* **108**, 191–206.

Sawford, B. L. 1983 The effect of Gaussian particle-pair distribution functions in the statistical theory of concentration fluctuations in homogeneous turbulence. *Quart. J. Roy. Met. Soc.* **109**, 339–354.

Sawford, B. L. 1985 Lagrangian statistical simulation of concentration mean and fluctuating fields. *J. Climate Appl. Met.* **24**, 1152–1166.

Sawford, B. L. 1991 Reynolds number effects in Lagrangian stochastic models of turbulent dispersion. *Phys Fluids* A **3**, 1577–1586.

Sawford, B. L. 2001 Turbulent relative dispersion. *Annu. Rev. Fluid Mech.* **33**, 289–317.

Sawford, B. L., Borgas, M. S. & Yeung, P. K. 2003 Lagrangian modeling of turbulent diffusion in the atmosphere – recent developments. In *Reynolds Number Scaling in Turbulent Flow* (ed. A. J. Smits), pp. 37–44. Kluwer.

Sawford, B. L. & Yeung, P. K. 2001 Lagrangian statistics in uniform shear flow: DNS and Lagrangian stochastic models. *Phys. Fluids* **13**, 2627–2634.

Sawford, B. L., Yeung, P. K., Borgas, M. S., Vedula, P., LaPorta, A., Crawford, A. M. & Bodenschatz, E. 2003 Conditional and unconditional acceleration statistics in turbulence. *Phys. Fluids* **15**, 3478–3489.

Shen, P. & Yeung, P. K. 1997 Fluid particle dispersion in homogeneous turbulent shear flow. *Phys. Fluids* **9**, 3472–3484.

Sreenivasan, K. R. 1995 On the universality of the Kolmogorov constant. *Phys. Fluids* **7**, 2778–2784.

Sreenivasan, K. R. & Antonia, R. A. 1997 The phenomenology of small-scale turbulence. *Annu. Rev. Fluid Mech.* **29**, 435–472.

Thomson, D. J. 1987 Criteria for the selection of stochastic models of particle trajectories in turbulent flows. *J. Fluid Mech.* **180**, 529–556.

Thomson, D. J. 1990 A stochastic model for the motion of particle pairs in isotropic high-Reynolds-number turbulence, and its application to the problem of concentration variance. *J. Fluid Mech.* **210**, 113–153.

Vedula, P. & Yeung, P. K. 1999 Similarity scaling of acceleration and pressure statistics in numerical simulations of isotropic turbulence. *Phys. Fluids* **11**, 1208–1220.

Voth, G. A., Satyanarayanan, K. & Bodenschatz, E. 1998 Lagrangian acceleration measurements at large Reynolds numbers. *Phys. Fluids* **10**, 2268–2280.

Weil, J. C., Sykes, R. I. & Venkatram, A. 1992 Evaluating air-quality models: review and outlook. *J. Appl. Met.* **31**, 1121–1145.

Yeung, P. K. 1994 Direct numerical simulation of two-particle relative diffusion in isotropic turbulence. *Phys. Fluids* **6**, 3416–3428.

Yeung, P. K. 1997*a* One- and two-particle Lagrangian acceleration correlations in numerically simulated homogeneous turbulence. *Phys. Fluids* **9**, 2981–2990.

Yeung, P. K. 1997*b* Two-time statistics of relative diffusion in direct numerical simulations of turbulence. *Proc. 12th Symp. Boundary Layers and Turbulence*, *American Meteorological Society, Vancouver, Canada*, pp. 223–224.

Yeung, P. K. 2001 Lagrangian characteristics of turbulence and scalar transport in direct numerical simulations. *J. Fluid Mech.* **427**, 241–274.

Yeung, P. K. 2002 Lagrangian investigations of turbulence. *Annu. Rev. Fluid Mech.* **34**, 115–142.

Yeung, P. K. & Borgas, M. S. 1998 Vector alignment properties of particle-pair dispersion in isotropic turbulence. *Proc. 13th Australasian Fluid Mech. Conf. Melbourne, Australia*, pp. 729–732.

Yeung, P. K. & Pope, S. B. 1988 An algorithm for tracking fluid particles in numerical simulations of homogeneous turbulence. *J. Comput. Phys.* **79**, 373–416.

Yeung, P. K. & Pope, S. B. 1989 Lagrangian statistics from direct numerical simulations of isotropic turbulence. *J. Fluid Mech.* **207**, 531–586.

Yeung, P. K., Xu, S., Borgas, M. S. & Sawford, B. L. 2003 Scaling of multi-particle Lagrangian statistics in direct numerical simulations. In *Reynolds Number Scaling in Turbulent Flow* (ed. A. J. Smits), pp. 163–168. Kluwer.

Yeung, P. K. & Zhou, Y. 1997 On the universality of the Kolmogorov constant in numerical simulations of turbulence. *Phys. Rev.* E **56**, 1746–1752.